ELECTRON TRANSFER KINETICS AND THERMODYNAMIC ACTIVATION PARAMETERS FOR SEVERAL AQUO COMPLEXES AT MERCURY-AQUEOUS INTERFACE

by

Sayed Muneebullah Husaini

A THESIS

Submitted to
Michigan State University
in partial fulfillment of the requirements
for the degree of

MASTER OF SCIENCE

Department of Chemistry

1982

ABSTRACT

ELECTRON TRANSFER KINETICS AND THERMODYNAMIC ACTIVATION PARAMETERS FOR SEVERAL AQUO COMPLEXES AT MERCURY-AQUEOUS INTERFACE

by

Sayed Muneebullah Husaini

A disparity was observed by Anson and Parkinson* between the electrocapillary data and kinetic results for electrochemical reactions about the double-layer structure in very dilute solutions of electrolytes at mercury-aqueous interface. This decrepancy was shown to emerge because of employing a potential independent transfer coefficient α = 0.5) to calcuate the double-layer potential ϕ_2 from kinetic results. The disagreement of results was resolved and experimentally investigated, for the oxidation reaction of Eu^{2+}_{aq} in different dilutions of various electrolytes, employing a potential dependent α.

The electrochemical redox reaction for $V^{3+/2+}_{aq}$ couple demonstrated a unique behavior among the transition metal redox couples by exhibiting a pH dependent reaction rate.

The activation parameters for the electrodeposition reaction for $Mn^{2+/0}_{aq}$, $Fe^{2+/0}_{aq}$, $Co^{2+/0}_{aq}$ and $Ni^{2+/0}_{aq}$ couples were determined in aqueous solutions. An increase in the activation entropy with increasing cathodic potential can be attributed to a partial desolvation of aqueous ligands at the mercury-aqueous interface.

---

*J. Electroanal. Chem., 85, 317 (1977).

In the name of God (Allah)
who is most merciful
most compassionate

ACKNOWLEDGEMENTS

Few words of thanks are like few drops of water returned to the ocean. All thanks to God who gave me the strength and courage to accomplish this work and who created a number of people who were helpful in my endeavor.

I owe a lot to Dr. Michael Weaver, my preceptor, who tried his best to bear with me despite my weaknesses.

I feel a great respect for Dr. Fredrick Horne who tried to help me out in difficult times.

My thanks are due to my parents, my brothers, sisters and wife, without their love and encouragement, I would not have been able to accomplish this task.

TABLE OF CONTENTS

TABLE OF CONTENTS (cont'd.)

LIST OF TABLES

LIST OF FIGURES

LIST OF FIGURES (cont'd.)

CHAPTER I

INTRODUCTION

Almost all chemical processes are primarily associated with the changes in the position and energy of electrons around the reacting nuclei. In an ordinary chemical reaction, these changes are influenced mutually by the reactant and product molecules or ions. An electrochemical reaction is different from an ordinary chemical reaction as it involves the passage of electrons through an external metal circuit provided with a voltage and current regulating device. Unlike ordinary electron transfer chemical reaction, where the electron donors and acceptors are molecules or ions, the metal or semi-conductor electrode surface acts as a reacting donor or acceptor of electrons in an electrochemical reaction. The electrochemical reaction has an advantage over an ordinary chemical reaction in that the electrode surface provides comparatively similar reaction conditions for a wide range of reaction species, while on the other side, the conditions for chemical reactions are limited by the availability of reactant ions or molecules.

The kinetic and thermodynamic parameters for an electrochemical reaction are heavily dependent on the structure of the solvent and reacting ions adjacent to the electrode surface. The concentration of reaction ions or molecules

does not remain the same near the electrode surface as in the bulk solution due to electrostatic as well as kinetic reasons[1-4]. The solvent molecules and sometimes other species (ions or molecules) present in solution, which sometimes are specifically adsorbed on the electrode surface, form a layer closest to the electrode surface; the locus of the electrical centers of the specifically adsorbed ions is called the inner Helmholtz plane (i.H.p.). Solvated "reactants" can reach closest to the metal electrode surface by touching the solvent molecules or adsorbed ions in the i.H.p. This distance is defined by the locus of the centers of these solvated reactants and is called the outer Helmholtz plane (o.H.p.). The part of the solution beyond the o.H.p. is called the diffuse layer (Figure 1.1). The structure of these layers, called the double-layer, and the distribution of potential in them has a great influence on the reaction kinetics and thermodynamic results[1-4]. The potential available for the reacting species, which can not approach the electrode surface closer than the o.H.p., is different from the applied potential at the electrode surface (Figure 1.2). Since the calculation of the reaction rate constant involves the value of potential experienced by the reacting ion, a precise knowledge of this quantity is highly needed. The distribution of the reactants closer to the reaction plane may not remain the same as in the bulk solution because of variation in coulombic attraction

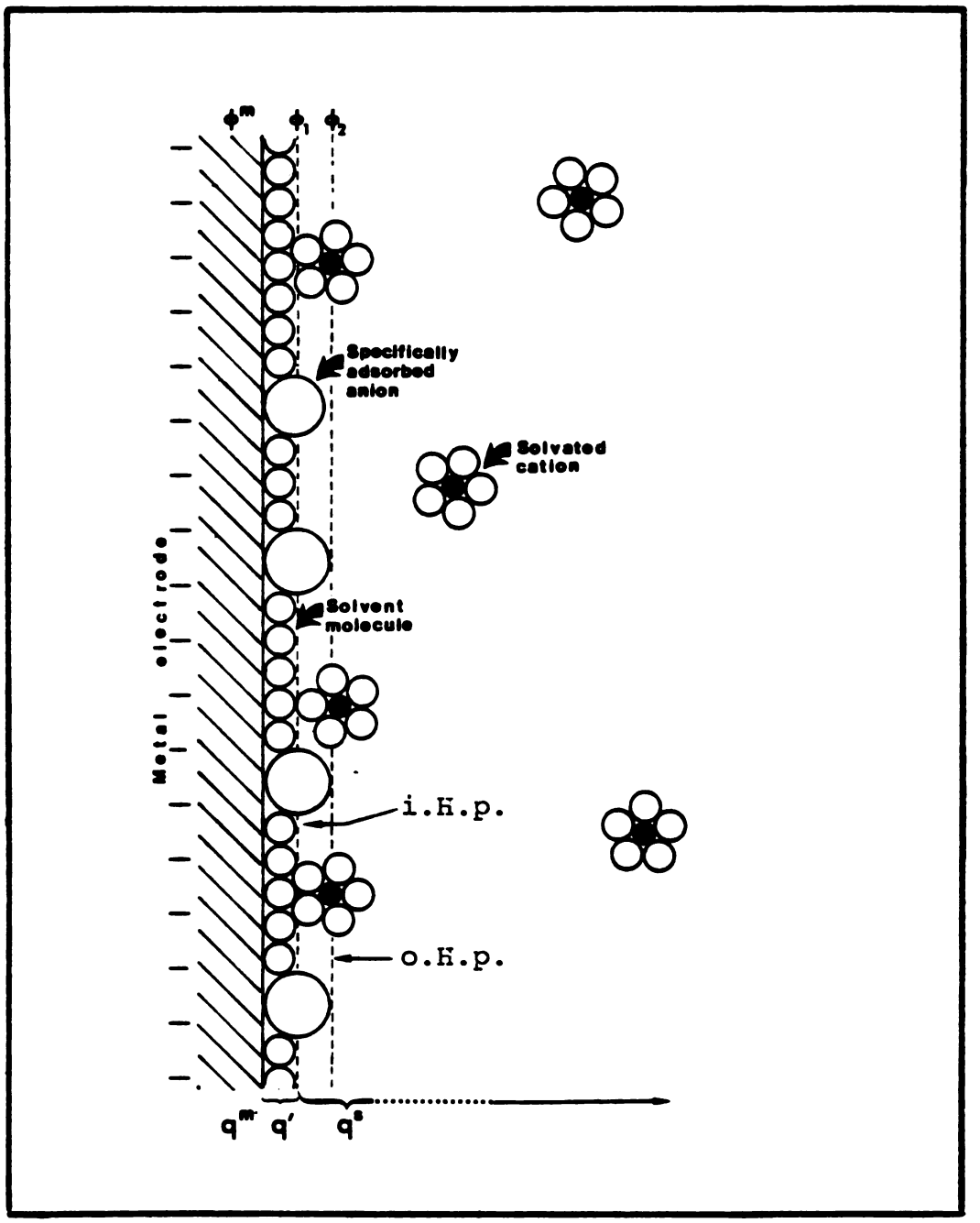

Figure 1.1. Double-layer structure at electrode-solution interphase.

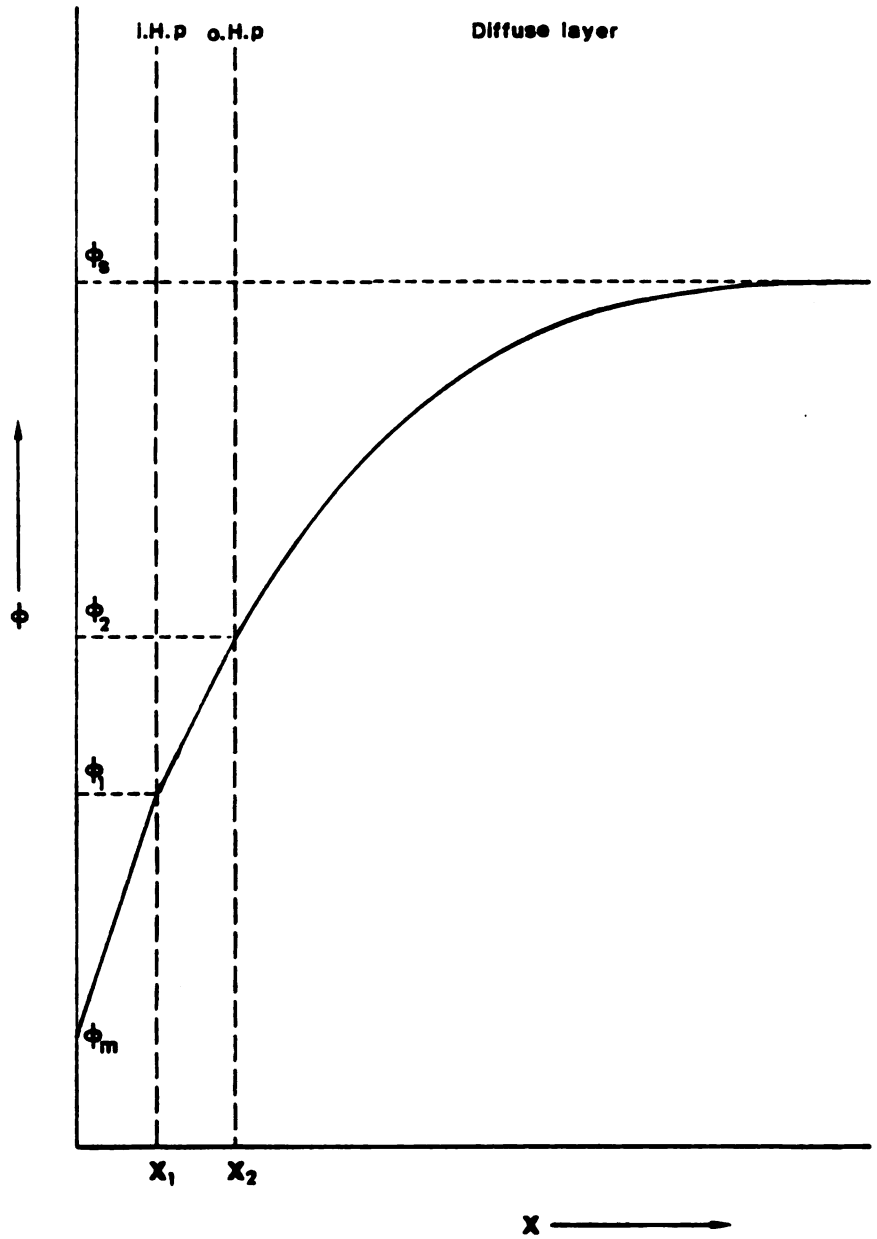

Figure 1.2. Potential-distance profile at the electrode-solution interphase according to Guoy-Chapman-Stern (GSC) model.

or repulsion of reactants with distance from the electrode surface, which, in turn, will also affect the kinetics of the reaction. These problems were successfully tackled by Frumkin[1-4] who formulated a correction to apply to the apparent (experimentally observed) rate constant, called the double-layer correction, which gives rate constant corrected for the variation of potential observed at the reaction site in the double-layer region. The Frumkin double-layer correction is commonly used throughout the electrochemical literature.

It was theorectically predicted that solutions at sufficiently high dilution of electrolyte would provide conditions in which given a positive potential at electrode, the anions from the supporting electrolyte would specifically adsorb in equal quantities to the positive electronic charge at the electrode metal[5, 6]. If the anionic and cationic charges were exactly matched, one might expect no diffuse layer to be present at any positive potential. The ironic result would be that one may avoid the Frumkin double-layer correction by using very low concentration of supporting electrolyte instead of high values (~ M) customarily employed to minimize the double-layer correction. This situation was further explored by Anson and Parkinson[5] who concluded, employing kinetic methods, that charged reactants behave in the way to be expected for dilute solutions if a diffuse layer were present at potentials where the previous non-kinetic measurement had suggested the contrary. The analysis

of their experimental results in electrolytes of low ionic strength using the Frumkin double-layer correction showed large discrepancies in the double-layer structure determined from kinetic and electrocapillary data with respect to as important a parameter as the sign of the potential difference across the diffuse layer.

The Frumkin double-layer correction performed by the authors for the analysis of their experimental results involved the construction of a hypothetical Tafel line*, assuming the absence of a diffuse layer, so that the diffuse layer potential ϕ_2, which was assumed to be the potential at the reaction site, became zero for all working potentials. The transfer coefficient α used to construct this Tafel line was assumed to be constant (0.5) for all working potentials. Those simple assumptions were further explored by Tyma and Weaver[7] who showed the transfer coefficient α to be dependent nonlinearly on the working potentials which give rise to a nonlinear Tafel line at $\phi_2 = 0$.

The experimental results of Anson and Parkinson[5], along with the results in this study using the same concentrations of electrolytes as well as other concentrations, were analyzed employing the Tafel lines at $\phi_2 = 0$ and the trarsfer coefficient α calculated by the authors as well as by Tyma and Weaver[7]. It was observed from the kinetic results that the extent of discrepancy between the charge on the

*A Tafel line is constructed by plotting logarithm of reaction rate versus potential for an electrochemical reaction.

metal and the total charge on the adsorbed ions, determined earlier by the analysis of the authors, were minimized and was shown to lie within the experimental range of error of the electrocapillary data. Their views about the GCS theory and, hence, the Frumkin double-layer correction arising from their kinetic results showing a large difference in charges between the metal and the absorbed ions were unduly pessimistic.

The electrochemical study of aquo metal complexes of transition metal ions in aqueous solution is often undertaken as a simple and basic working system, because most of the kinetic and thermodynamic parameters for their homogeneous analogs are well established. It is generally assumed while working with the aquo complexes of metal ions in aqueous solution that these simple electron reactions will not have any influence due to a variation in the H^+ ion concentration. These reactions are usually studied without checking the pH dependence of reaction kinetics.

In the second part of the thesis, pH dependence of the electrochemical reaction rates of various $M^{3+/2+}$ and $M^{2+/0}$ aquo couples were examined using polarographic and cyclic voltammetric techniques. It was found that the electrochemical reaction rate for $V^{3+/2+}$ couple only behaved differently and was dependent on pH while the rest of the couples exhibit no pH dependence. This situation becomes more important because a number of research papers on the

electrochemical kinetics have been published using $V^{3+/2+}$ couple assuming it to be pH independent.

The third part of the thesis, which is experimentally the longest part, deals with the thermodynamic activation parameters for electrodeposition reactions of several metals from the first transition series. The activation parameters contribute information which often proves helpful in understanding and interpreting the kinetics of reactions. Study of the temperature dependence of chemical reaction rate constants is used as a well established procedure in chemical kinetics to determine the activation parameters of the reaction. Surprisingly few people have tried to determine the "electrochemical" activation parameters using the temperature dependence of electrode reaction rates. This neglect is due to a common belief that it is a non-measurable quantity in the experimental set-up of electrochemical reactions, where the electrical state at the reaction site does not remain constant while altering the temperature of the system[4, 8-12]. This problem has been fully discussed and it is concluded that the "real" activation parameters derived from the temperature dependence of the "standard" electrochemical rate constant are closely related to the entropy and enthalpy of the corresponding self-exchange reactions[9]. For electrochemically irreversible process where the standard potential in unknown and so are the "real" activation parameters, the "ideal" activation parameters are still

derivable quantities[8]. These quantities can be obtained from the temperature dependence of the electrochemical rate constant when the metal-solution Galvani potential difference ϕ_m is held constant[9]. These parameters represent the actual enthalpic and entropic barrier heights for the single reacting species at the electrode potential at which they are determined.

An important class of electrochemical reactions, the electrodeposition reaction of metals, where the metal ion is completely reduced to metal atom, was selected to be studied in relation with their activation parameters in aqueous solution. Aquo complexes of several metals from the first transition series which provides irreversible systems were selected for the study of activation parameters of these reactions. These reactions are expected to give valuable information about kinetics and mechanism, where the reduced species is not an ion but a solid uncharged particle. The values of the activation parameters were analyzed and discussed in relation to their reaction mechanisms.

CHAPTER II

EXPERIMENTAL METHODS

This chapter deals with the apparatus and reagents employed in most of the electrochemical experiments.

A. Materials

1. Solvent (water)

The water utilized as solvent was purified by passing the general purpose distilled water through a "Milli-Q" purification system (Millipore Corporation) consisting of a set of ion-exchange units and an activated charcoal filter. This water was assumed to be adequate for the experimental work performed at mercury electrode.

2. Oxygen Removal

The presence of dissolved oxygen from atmosphere in solution was removed by bubbling purified nitrogen through the solution just prior to starting the experiment.

3. Electrolytes

All electrolytes utilized in the experiments were recrystallized in pyrodistilled water. Sodium perchlorate was prepared by allowing sodium carbonate to react with 60% perchloric acid.

4. Reactant solutions

$Eu(H_2O)_6^{3+}$ was prepared by dissolving Eu_2O_3 in equivalent amounts of $HClO_4$ solution and diluting with appropriate amounts of water. $Eu(H_2O)_6^{2+}$ was prepared by exhaustive electrolysis of $Eu(H_2O)_6^{3+}$ at -900 mV vs. s.c.e. $V(H_2O)_6^{2+}$ was prepared by similar method using V_2O_5 as starting material, and an applied voltage of -1100 mV vs. s.c.e. This solution was further oxidized to $V(H_2O)_6^{3+}$ by electrolysis at -600 mV vs. s.c.e. The aqueous solutions of Mn^{2+}, Fe^{2+}, Co^{2+} and Ni^{2+} were prepared by dissolving the perchlorate of these ions in water.

B. Apparatus

1. Electrochemical Cell

The electrochemical cell was a conventional two component jacketed design made of pyrex glass with two "very fine" frits made by Corning, Inc. (average porosity 1-3μm) separating the working, reference, and counter electrode in different compartments and inhibiting the mixing of solution in different compartments. The cell was cleaned for each experiment by leaving it for 48 hours in a concentrated chromic acid cleaning solution followed by washing with distilled water and then leaving it again for 48 hours in distilled water to ensure complete removal of any trace of chromic acid. The cell was next left in the oven at ~200°C overnight and then wrapped in plastic sheets after cooling.

2. Reference electrode

Commercial (Sargent-Welch) reference electrodes were used for the electrochemical measurements. The sodium saturated calomel electrode (NaSCE) was prepared by replacing KCl with NaCl. Appropriate corrections to the value of applied voltage were made when using NaSCE.

3. Polarographic Instrument

DC and normal pulse polarography and cyclic voltammetry were performed using a Princeton Applied Research Model 174 (PAR 174) polarographic analyser with a Hewlett-Packard 7045A X-Y recorder. Water was circulated around the working compartment and the liquid junction using a thermostat water circulator. The temperature could be varied from 0°C to more than 60°C and served the purpose of our experimental range. The temperature of the solution the working compartment was measured using a precise thermometer which could be read within ±0.5°C. The temperature of the compartment of reference electrode was kept fixed at ambient room temperatures, usually 23 ± 0.5°C.

C. Electrochemical Techniques

1. DC and pulse experiments were done using a dropping mercury electrode having a constant mercury flow rate at constant temperature and a time dependent drop knocker. The glass tip of the dropping mercury working electrode was

sufficiently immersed in the solution to ensure efficient heating of the mercury drop while performing the activation parameter experiments. The variation of the mercury flow rate with temperature was also determined for the use in the analysis of activation parameter experiments. The polarograms for DC polarography were analyzed employing Koutecky analysis[13, 14], while Parry-Oldham analysis[15] was carried out for normal-pulse polarography.

2. Cyclic voltammetry was done using a micrometer type hanging mercury drop electrode (HMDE) with an adjustable drop size. The sweep rates used were within a range of 20-500 mV s^{-1}. The analyses of quasi-reversible electrode reactions were done utilizing the method outlined by Nicholson[16].

CHAPTER III

DOUBLE-LAYER STRUCTURE IN DILUTE ELECTROLYTES

A. Double-Layer Structure and Electrode Kinetics

When a metal electrode surface is brought in contact with a solution, the electrical charge on the metal due to electrode potential causes oppositely charged ions to accumulate on the solution side of the interface called the "electrical double-layer". The presence of this electrical double-layer results in a nonlinear distribution of electrical potential and solution composition near the electrode surface. The knowledge of this distribution is very important for an understanding of electrode kinetics because the reaction rates are sensitive to changes in potential at the electrode-solution interface and also to the concentration of reacting ion next to the electrode. The first and simplest model for the double-layer structure was proposed by Helmholtz[1-4]. According to Helmholtz, the double-layer may be regarded as ions attracted towards the electrode surface forming a compact layer at a fixed distance from the electrode surface. This situation can be regarded as equivalent to an electrical parallel-plate condenser, one plate of which coincides with the plane passing through the surface charges in the metal and the other with the plane

connecting the center of ions residing in the solution but attracted to the metal surface by electrostatic forces. By the law of electroneutrality, which also holds for the phase boundary, the ions drawn to the metal surface must precisely compensate the surface charges of the metal. This structure does not account for the experimentally observed change in the capacity with potential and with ion concentration in solution. The Helmholtz theory is thus incapable of providing a satisfactory interpretation of the basic experimental regularities associated with the double-layer structure, and hence needs a modification. The Helmholtz theory also does not take into account the change in properties of the double layer with temperature.

Guoy and Chapman made an attempt to eliminate this weakness of the Helmholtz theory by relating the charge density in the double-layer to the solution composition. They noted that the strictly fixed array of ions postulated in the parallel plate model is in fact impossible because, apart from the electrostatic forces arising between the metal and the ions, the latter are also acted on by forces of thermal molecular motion. Under the combined effects of these forces, the excess ions are distributed diffusely rather than compactly next to the electrode surface. For this structure of the double-layer, one cannot make use of the formula for a parallel-plate condenser to express the relation between the charge density and potential. In

order to find the charge distribution in the solution as a function of potential, some definite assumption were needed to be made on the law of its variation with distance from the electrode surface. Guoy and Chapman maintained that the ions could be viewed as material points having no volume but possessing a definite charge and that their distribution in the field of the charge smeared uniformily over the electrode surface obeying the Botlzmann formula. The starting point to determine the variation of the charge density with respect to distance from the electrode are the Boltzmann and Poisson equations. This problem is treated by analogy with Debye-Hückel theory which calculates the variation of potential and distribution of ions around a central ion -- a spherically symmetrical problem.

The Guoy-Chapman theory, although it is best justified where the Helmholtz model is found to be inadequate, failed to predict accurately the variation of double-layer capacitance with respect to applied potential. The discrepancy with experimental values becomes even more pronounced for concentrated solutions where the Helmholtz model gives better results.

Stern proposed a structure for the double-layer in his adsorption theory as a combination of Helmholtz and Guoy-Chapman model. According to Stern's picture, some of the ions in solution stick to the electrode, forming the Helmholtz sheet of double-layer with a thickness corresponding to the average radius of the ions attracted towards the

electrode surface, called the outer Helmholtz plane (o.H.p.). The remaining ions form an ionic atmosphere of the electrode diffusely spread out with decreasing charge density, where there is a balance between the electrostatic forces and the thermal random motions (Figures 1.1 and 1.2). This model can be expressed as two capacitors in series, one representing the capacitance of the outer Helmholtz layer and the other, the capacitance of the diffuse double-layer. Additionally, Stern suggested that, in the Helmholtz region, the ions are held out not only by electrostatic forces but also by forces of specific adsorption which are of non-Coulombic origin.

Although the Stern's modification of Helmholtz and Guoy-Chapman theory provides better agreement of experimental results with the theoretical values, Stern still neglected the size of the ions in the diffuse portion of double-layer. The theory of the double-layer structure was further developed in the work of Frumkin and his school and also by Grahame, Parson, Devanathan and other workers[1-4]. According to them, an inner Helmholtz plane which resides inside the outer Helmholtz plane and is composed of specifically adsorbed ions, partly or completely hydrated, attached immediately next to the electrode surface (Figure 1.1) should be included. The o.H.p. contains hydrated ions drawn to the metal surface by electrostatic forces. It is observed that this model of the double-layer has numerous advantages over Stern's presentation. It brings the theoretical results closer to experimental values[1-4].

B. Frumkin Double-Layer Correction

After obtaining a description for the variation of potential with distance close to the electrode surface, the effect of this relationship on electrode kinetics was the next problem to be studied. This problem was successfully handled by the Russian scientist, A.N. Frumkin[1-4]. According to his proposal, molecules or ions in the diffuse layer are too far away from the electrode surface to react and they have to be brought at least to the o.H.p. for the electron transfer. The concentration may well be different at the o.H.p. than in the bulk solution. This situation can be shown in an electrochemical reaction as:

$$Ox_* \rightleftharpoons Ox_{\neq} + ne^-(\phi_{\neq}) \underset{k_{-1}}{\overset{k_1}{\rightleftharpoons}} Red_{\neq} \rightleftharpoons Red_* \qquad (3.1)$$

where Ox_* and Red_* show the concentrations of oxidant and reductant just outside the double-layer whereas $Ox_{\neq}$ and $Red_{\neq}$ represent the concentration of oxidant and reductant at the right distance from the electrode for the electron exchange reaction. $\phi_{\neq}$ represents the potential available at the reacting site which can be roughly assumed to be the o.H.p. Work is thus needed to bring the particle from outside the o.H.p. or to take the particle away from the o.H.p. into the bulk solution. This work originates from the interaction of charge on the particle with the field it experiences. According to a very simple model, an ion carrying z total charge, considered as spherically distributed, will need work W to bring it to the position of closest approach.

W is given by:

$$E = zF(\phi_{\neq}) \tag{3.2}$$

The concentration of oxidant and reductant at reaction site using the Boltzman distribution law

$$[O_{\neq}] = [O_{*}] \exp \left[\frac{-z_o F(\phi_{\neq}-\phi_s)}{RT}\right] \tag{3.3}$$

$$[R_{\neq}] = [R_{*}] \exp \left[\frac{-z_R F(\phi_{\neq}-\phi_s)}{RT}\right] \tag{3.4}$$

where z_0, z_R are the charges on the oxidant and reductant and ϕ_s is the potential in the bulk of the solution. F, R and T have their usual meanings.

According to the electrochemical rate equation:

$$\ln k_1 = \ln k_1^o - \frac{\alpha_{corr} nF(\phi_M-\phi_{\neq})}{RT} \tag{3.5}$$

where k_1 is the rate of the forward reaction at any potential, and k_1^o is the standard rate constant, α_{corr} is the corrected transfer coefficient and ϕ_M is the potential at the metal electrode surface. Similarly the rate of backward reaction,

$$\ln k_{-1} = \ln k_{-1}^o + \frac{(1-\alpha_{corr})nF(\phi_M-\phi_{\neq})}{RT} \tag{3.6}$$

The rate of the forward reaction $Ox_* \longrightarrow Red_*$, is

$$(Rate)_1 = k_1[O_{\neq}] = k_1^o \exp \left[\frac{\alpha_{corr} nF(\phi_M-\phi_{\neq})}{RT}\right] \cdot [O_{\neq}]; \tag{3.7}$$

substituting $[O_{\neq}]$ from (3.3)

$$(Rate)_1 = k_1^o \exp \left[\frac{-\alpha_{corr} nF(\phi_M-\phi_{\neq})}{RT}\right] \exp \left[\frac{-zF(\phi_M-\phi_s)}{RT}\right] \cdot [O_{*}]. \tag{3.8}$$

Rearranging

$$(\text{Rate})_1 = k_1^o \exp\left[\frac{-\alpha_{corr} nF(\phi_M-\phi_{\neq})}{RT}\right] \cdot \exp\left[\frac{(\alpha n_{corr}-z_o)F(\phi_M-\phi_s)}{RT}\right] \cdot [0_*] \qquad (3.9)$$

Defining f_{DL}, the double-layer correction factor, as

$$f_{DL} = \exp\left[\frac{(\alpha_{corr} n-z_o)F(\phi_{\neq}-\phi_s)}{RT}\right], \qquad (3.10)$$

$$(\text{Rate})_1 = k_1^o \exp\left[\frac{-\alpha_{corr} nF(\phi_M-\phi_s)}{RT}\right] f_{DL}[0_*] \qquad (3.11)$$

where $(\phi_M-\phi_s)$ can be measured by changing the potential difference of the whole cell.

Similarly, for the backward reaction,

$$(\text{Rate})_{-1} = k_{-1}^{\hat{o}} \exp\left[\frac{(1-\alpha_{corr})nF(\phi_M-\phi_s)}{RT}\right] f_{DL}\ [R_*] \qquad (3.12)$$

where f_{DL} is the same as for the forward reaction.

Equations (3.5) and (3.8) can be compared and rearranged to give a rate constant corrected for the double-layer as

$$k_1^E = k_1^E(corr) \exp\left[\frac{(\alpha n_{corr}-z_o)F\phi_{\neq}}{RT}\right] \qquad (3.13)$$

and $$k_{-1}^E = k_1^E(corr) \exp\left[\frac{(\alpha_{corr} n+z_R)F\phi_{\neq}}{RT}\right] \qquad (3.14)$$

where k_1^E, k_{-1}^E are the rate constants at any potential E.

The correction proposed by Frumkin proved to work successfully when applied to a number of electrochemical problems and it works well for the reactions. However, the application of these corrections is most straightforward in absence of specific ionic adsorption; it becomes complicated in the presence of specific ionic adsorption because the potential at the reaction site, $\phi_{\neq}$, which appears in the Frumkin correction, is influenced by the amount of the charged specific adsorption on the electrode surface[1-4].

C. Verification of Double-Layer Structure in Dilute Solution

It was suggested[5,6] that at sufficiently high dilutions ($\sim 10^{-2}$ or less), the solution containing the adsorbing ion will exactly counterbalance the charge on the metal electrode, and hence, will give zero potential at the o.H.p. at all potentials positive of p.z.c. In this situation one can avoid the Frumkin double-layer correction when dealing with kinetic problems.

Anson and Parkinson[5] in their paper verified this assumption and, with the help of electrocapillary data, confirmed the presence of specific adsorbed ions with total charge equal to the charge on the metal electrode.

This situation was experimentally checked by the authors utilizing the kinetic method, since it is well established that the reaction rates are greatly influenced by the structure of the double-layer according to the Frumkin

double-layer correction.

$$k_1^E = k_1^E(\text{corr}) \exp\left[\frac{(\alpha_{\text{corr}} n - z_o) F \phi_{\neq}}{RT}\right] \qquad (3.15)$$

According to the non-kinetic measurement, since the charge on the metal is exactly balanced by the specific adsorbed ions, one would expect no diffuse layer, the potential at the reacting site $\phi_{\neq}$ should be zero, and hence $k_{-1}^E = k_1^E(\text{corr})$; this implies that there is no need to use the double-layer correction.

The kinetic probes used by the authors were the oxidation reactions of very dilute solutions (0.2m$\underline{M}$) of Eu^{2+} and V^{2+} ions in dilute concentrations of $HClO_4$, HCl and HBr electrolytes. The authors constructed a hypothetical Tafel line (log k^E vs. E) assuming $\phi_2 = 0$ at all potentials thus implying the non-existence of any diffuse layer, where ϕ_2 is the potential at the o.H.p. This $\phi_2 = 0$ line for $Eu^{3+/2+}$ couple was constructed from the standard potential (-620 mV vs. s.c.e.) in 1 m$\underline{M}$ $HClO_4$, the standard rate constant, and the transfer coefficient (0.5)[17, 19].

The ϕ_2 values were calculated by assuming the potential at the reaction site $\phi_{\neq}$ to be roughly equal to ϕ_2, the double-layer potential at the o.H.p. The calculations were performed using the equation

$$\ln k_{\text{app}} - \ln k_{\text{corr}} = \frac{(\alpha_{\text{corr}} n + z_R) F \phi_2}{RT} \qquad (3.16)$$

where k_{corr} were the values obtained at different potentials from the hypothetical Tafel line at $\phi_2 = 0$. With $z = 2$ and $\alpha_{corr} = 0.5$ at 25°C,

$$\phi_2 = 23.6 \ (\log k_{app} - \log k_{corr}). \qquad (3.17)$$

The values of ϕ_2 obtained in this manner for 0.2 m$\underline{M}$ Eu^{2+} oxidation reaction in 1.55 m$\underline{M}$ $HClO_4$, 0.8 m$\underline{M}$ HCl and 0.48 m$\underline{M}$ HBr were plotted against the potential vs. s.c.e. The authors concluded from these plots that the adsorption of anions from the percholrate, chloride and bromide electrolytes does not cause the potential experienced by the reactant to decrease to zero as assumed in the previous electrocapillary charge-potential data[6].

It was shown by Tyma and Weaver[7] that the assumption for transfer coefficient to be independent of the applied potential is not valid[7]. Thus the variation of α with potential would influence the hypothetical Tafel line for Eu^{2+} at $\phi_2 = 0$ to be curved instead of being linear as assumed earlier[5]. The kinetic results of Anson and Parkinson[5] were analyzed for ϕ_2 values using the Tyma and Weaver[7] Tafel line at $\phi_2 = 0$ and the corrected values of the transfer coefficient α. The results obtained above were also plotted against applied potentials.

In the present work, the experimental results of Anson and Parkinson[5] were analyzed and plotted for E vs. ϕ_2 and E vs. the excess charge of the adsorbed ions, calculated from

the GCS theory, and the excess charge in the diffuse layer, utilizing both methods outlined above. The experiments were performed again using the same concentrations and utilizing both methods of analysis. Several other experiments were performed using the same concentration of Eu^{2+} (0.2 m$\underline{M}$) but employing increased concentrations of the supporting electrolytes. The results were analyzed for ϕ_2 and the excess charge on the solution side and plots were obtained for these quantities vs. the electrode potential.

D. Experimental Procedure and Analysis of Data

Solutions of 0.2 m$\underline{M}$ Eu^{2+} were prepared in 1.55 m$\underline{M}$, 4.0 m$\underline{M}$ and 7.5 m$\underline{M}$ $HClO_4$, 0.8 m$\underline{M}$, 2.0 m$\underline{M}$, 4.0 m$\underline{M}$ and 20.0 m$\underline{M}$ HCl, and 0.48 m$\underline{M}$, 1.2 m$\underline{M}$ and 2.4 m$\underline{M}$ HBr as supporting electrolytes. DC polarography was employed for the oxidation reactions of these solutions and for the supporting electrolytes separately at constant ambient temperature (23 ± 0.5°C). The height of the mercury pool was kept at 50cm and the drop time was 1 second throughout all experiments. NaSCE was utilized for all experiments as the reference electrode to prevent the likely precipitation of $KClO_4$ if KSCE were used. Polarograms of current versus potential for these solutions were obtained along with the polarograms for the supporting electrolytes only. The current versus potential data were tabulated after subtracting the non-Faradaic current contributed by supporting electrolytes. The data

were analyzed for the apparent rate constant versus potential using diffusion coefficients for Eu^{2+} as 7.6×10^{-6} $cm^2.S^{-1}$[20]. These results were plotted against potential (as well as the Tafel lines at $\phi_2 = 0$ tabulated by Anson and Parkinson[5] and Tyma and Weaver[7] (Figures 3.2-3.5)). The values for the Tafel plots at $\phi_2 = 0$ by the above authors were corrected for the difference caused by using NaSCE instead of KSCE. This correction was determined to be 20 mV by comparing the relative potentials, utilizing a potentiometer in the same range of concentrations. The results obtained by Anson and Parkinson[5], corrected for NaSCE as reference electrode, were also plotted as above (Figure 3.1). The two sets of experimental results match within experimental error. ϕ_2 values for all these plots were calculated according to the equation 3.15 in the previous section. Two sets of data were obtained using each of the k_{corr}, constructed at $\phi_2 = 0$, by Anson and Parkinson[5] and Tyma and Weaver[7]. These results of ϕ_2 and the corresponding excess charge on the solution side calculated utilizing the GCS theory were also plotted against the potential (Figures 3.6-3.25).

E. Results and Discussion

The speculation of Anson and Parkinson and others[5, 6] that it might be possible to eliminate the diffuse layer by utilizing sufficiently dilute solutions of specifically adsorbed anions proved to be unrealistic based on their

calculation utilizing combination of Guoy-Chapman-Stern (GSF) Theory[2] and the Frumkin equation[36] (the "GCSF prediction"). It was assumed that when the specifically adsorbed anions exactly counterbalanced the electronic charge on the metal electrode ($q^m + q' = 0$), the potential at the reaction plane ϕ_{rp} (which can be to a very good approximation assumed to be equal to ϕ_2, the potential at the o.H.p. appearing in the GCS theory) would be essentially zero, and hence it would not be necessary to resort to the Frumkin double-layer correction.

The above assumption was tested using the kinetic method employing the Eu^{2+}_{aq} oxidation reaction; by constructing a hypothetical Tafel line at $\phi_2 = 0$[5]; according to the assumption of Anson and Parkinson[5] the kinetic results should lie on the hypothetical Tafel line i.e., the values obtained if Eu^{2+}_{aq} ion experiences no diffuse layer. The hypothetical Tafel line was constructed assuming the anodic transfer coefficient α to be 0.5.

The prediction of contemporary electron transfer theories[30, 37] that the electrochemical transfer coefficient α for outer sphere electrode reaction should depend upon the electrode potential[38, 39, 40] has been experimentally verified. It has been shown that the apparent transfer coefficient α_{app} for an electrochemical reaction often varies markedly with electrode potential as a result of ionic double-layer effects. The dependence of measured

(apparent) transfer coefficients upon electrode potential generally differs from that of the required "intrinsic" transfer coefficient α_I [49] as a result of the influence of the interphasial environment ("double-layer" effects). Tyma and Weaver [7] calculated the intrinsic transfer coefficient for the Eu^{2+}_{aq} oxidation reaction using a harmonic oscillator model and also determined semi-quantitative estimates of α_{corr}. The apparent transfer coefficient was corrected for double-layer effects using the equation

$$\alpha_{corr} = \frac{\alpha_{app} + z_r (\partial\phi_{rp}/\partial E)_\mu + \phi_{rp} (\partial\alpha_{corr}/\partial E)_\mu}{1 - (\partial\phi_{rp}/\partial E)_\mu} \qquad (3.18)$$

where z_r is the reactant charge, ϕ_{rp} is the average potential on the reaction plane, and μ is the chemical potential. They constructed the corrected Tafel line using

$$(\alpha_I)_{calc} = 0.5 \pm F(E_f - E)/2\lambda, \qquad (3.19)$$

where λ is the Marcus intrinsic reorganization term; λ is related to the double-layer corrected rate constrant k_{corr} at the formal (standard) potential E_f by [31]

$$RTm(k^s_{corr}/z) = -\lambda/4, \qquad (3.20)$$

where z is the heterogeneous collision frequency. Usually z is calculated from $z = (kT/2\pi m)^{\frac{1}{2}}$, where m is the effective mass of the reactant.

It was found that the experimentally corrected Tafel plots clearly exhibit more curvature than the theorectical

plots at anodic overpotentials for the Eu^{2+}_{aq} system.

The curved Tafel line shown in Figures 3.1 to 3.5 obtained by Tyma and Weaver[7] along with the Tafel line used by Anson and Parkinson[5] clearly shows that the deviation of the experimentally observed rate constants from the expected values (Tafel line at $\phi_2 = 0$) for the former case is substantially less than the latter case. The values of ϕ_2 for each system were calculated using the above plots and Frumkin double-layer correction[2] and are plotted in Figures 3.6 to 3.15 for all concentrations in each supporting electrolyte. These plots show that the double-layer potential ϕ_2 expected from the GCSF prediction for the reactions using Anson and Parkinson's Tafel plot are much larger than the values obtained using corrected Tafel line. The plots for the total excess charge on the solution side for these ϕ_2 values (obtained from each method of calculation) versus potential clearly demonstrate that the results obtained using Anson and Parkinson's constructed Tafel line (Figures 3.16, 3.18, 3.20, 3.22, 3.24) give roughly three to five times higher values than those obtained from the corrected Tafel line constructed by Tyma and Weaver (Figures 3.17, 3.19, 3.21, 3.23, 3.25).

The basis of the argument given[5] to question the correction of the GCSF prediction was the magnitude of ϕ_{rp} obtained from the dynamic (kinetic) method as compared to ϕ_2 values obtained from the static (electrocapillary data) method. The calculations performed in this

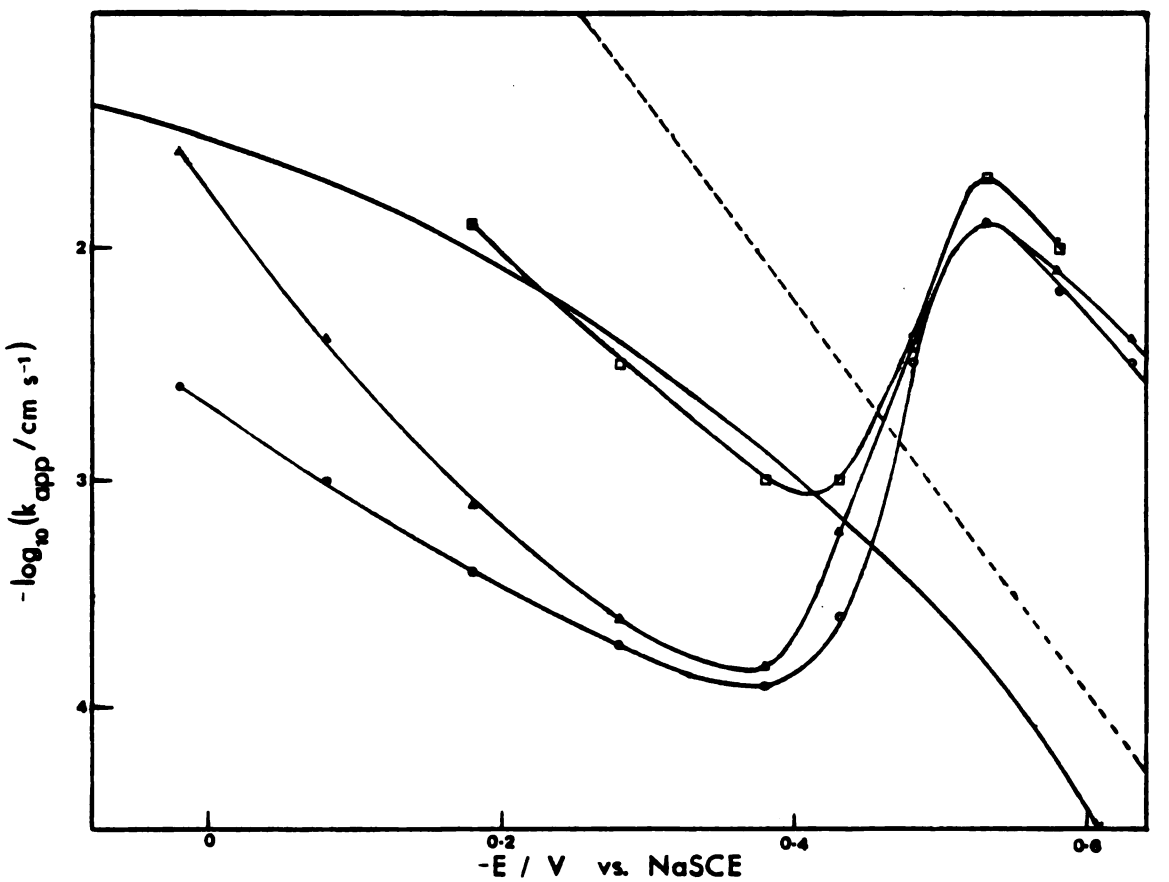

Figure 3.1. Rate-potential data from Anson and Parkinson[5] for the oxidation of 0.2 mM Eu^{2+} in aqueous solutions of various electrolytes: 1.55 mM $HClO_4$ (circles); 0.8 mM HCl (triangles); 0.48 mM HBr (squares). Also Tafel lines at ϕ_2 from Anson and Parkinson[5] (dashed line) and from Tyma and Weaver[7] (solid line).

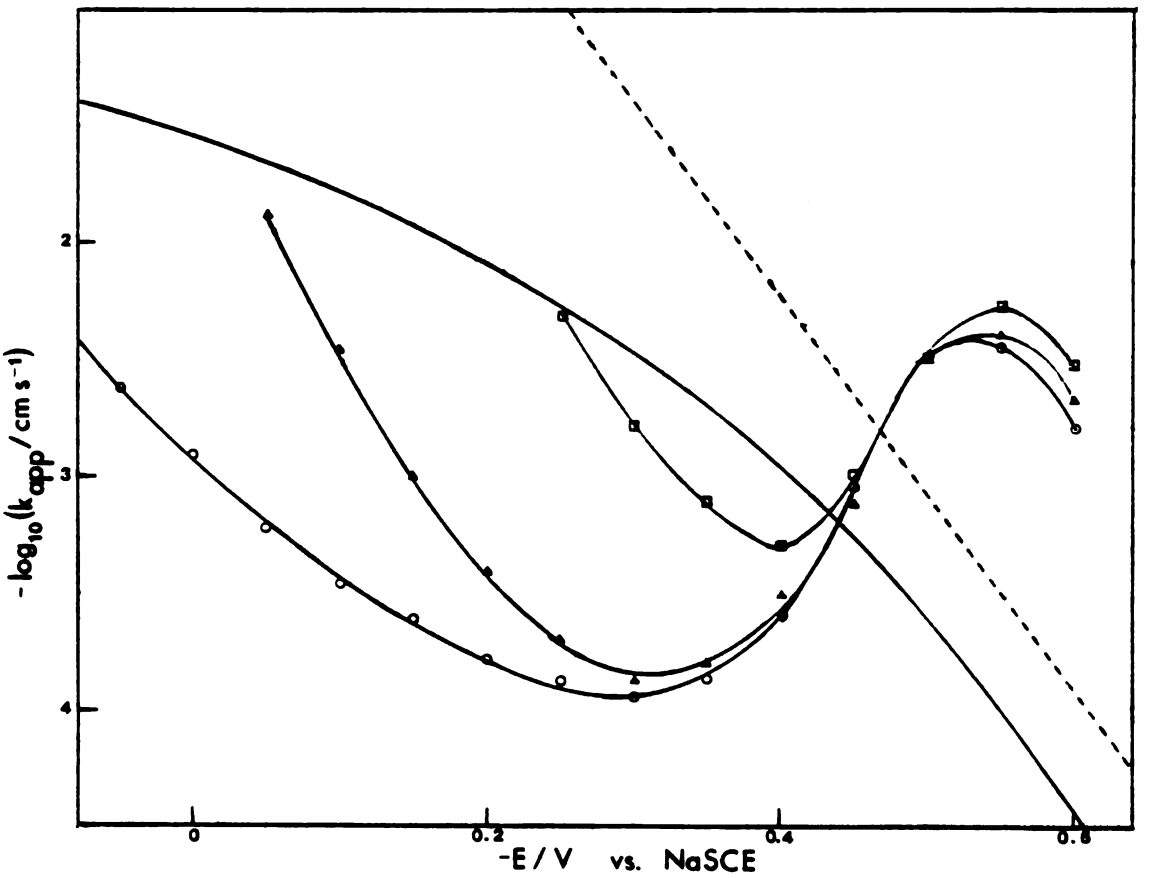

Figure 3.2. Rate-potential data for the oxidation of 0.2 mM Eu^{2+} in aqueous solutions of various electrolytes: 1.55 mM $HClO_4$ (circles); 0.8 mM HCl (triangles); 0.48 mM HBr (squares); Tafel lines at $\phi_2 = 0$ from Anson and Parkinson[5] (dashed line) and from Tyma and Weaver[7] (solid line).

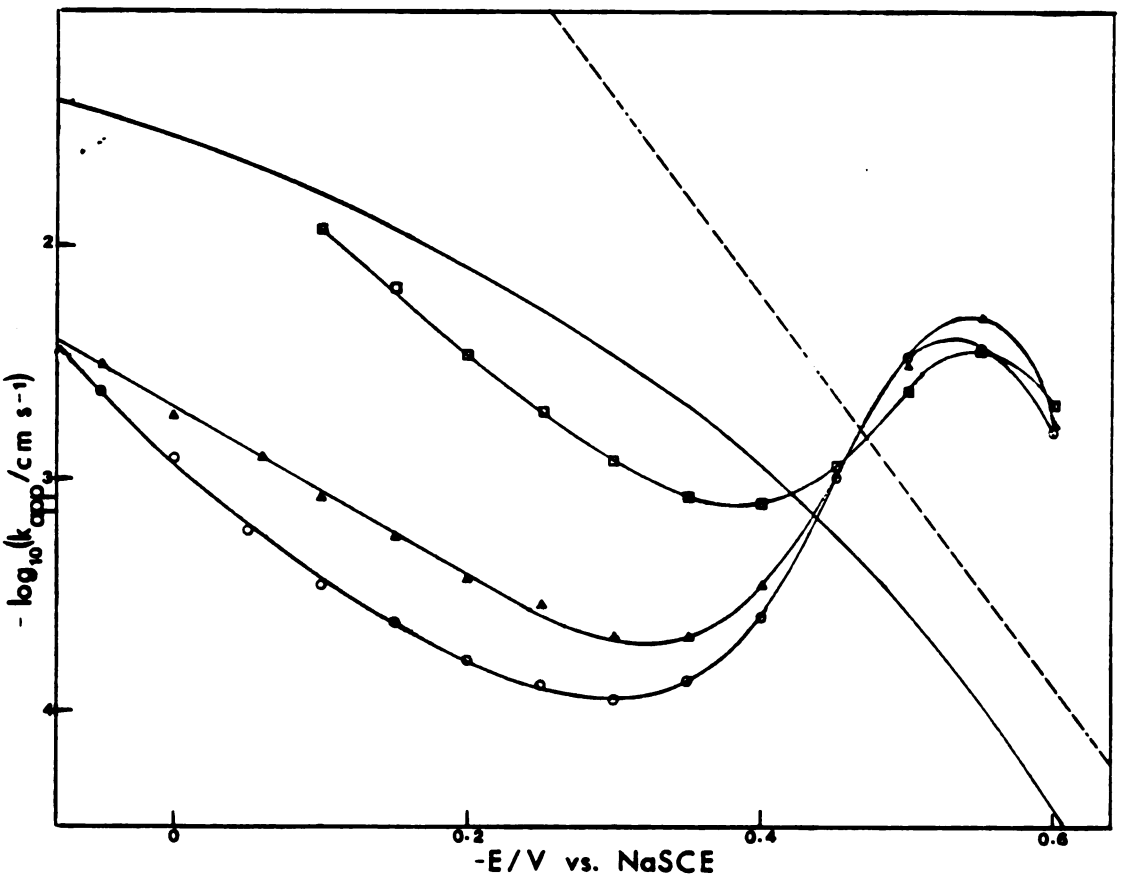

Figure 3.3. Rate-potential data for the oxidation of 0.2 mM Eu^{2+} in aqueous solutions of $HClO_4$: 1.55 mM (circles); 4.0 mM (Triangles); 7.75 mM (squares). Also Tafel lines at $\phi_2 = 0$ from Anson and Parkinson[5] (dashed line) and Tyma Weaver[7] (solid line).

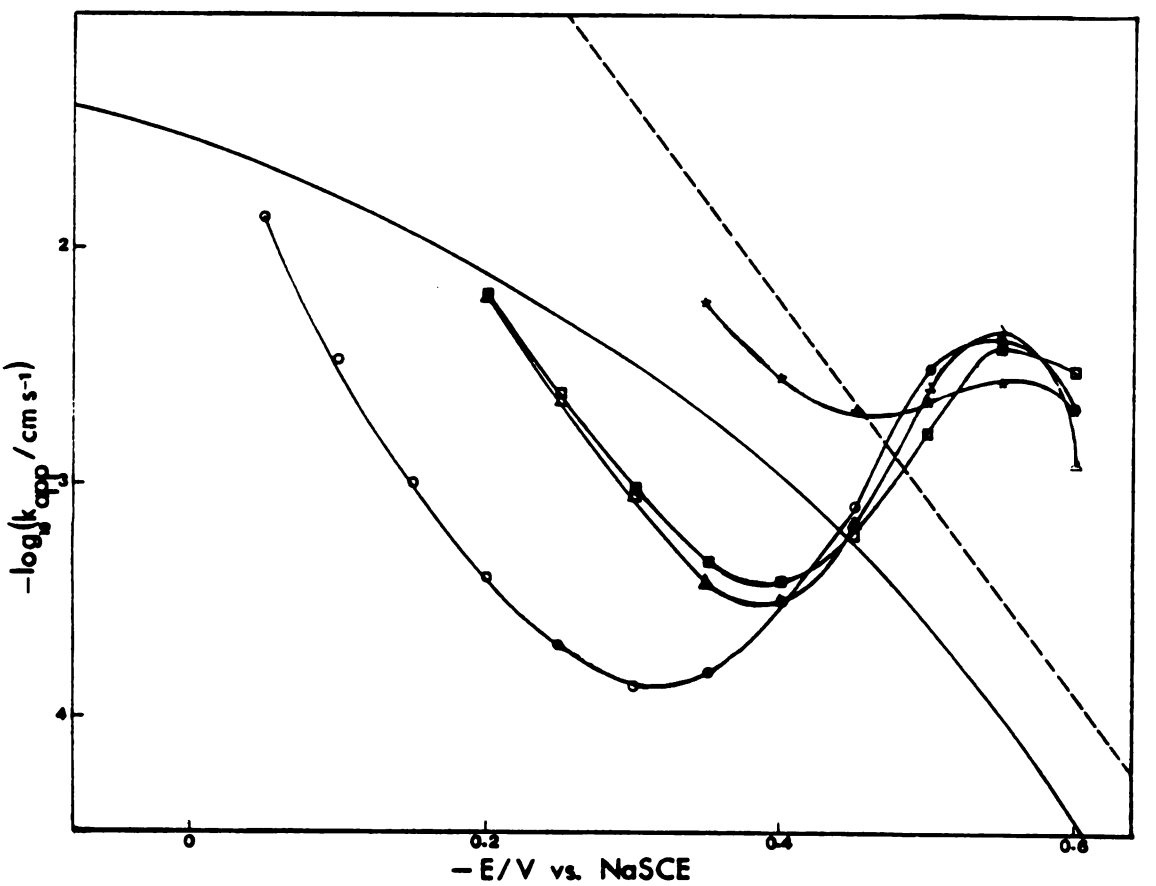

Figure 3.4. Rate-potential data for the oxidation of 0.2 mM Eu^{2+} in aqueous solutions of HCl: 0.8 mM (circles); 2.0 mM (triangles); 4.0 mM (squares); 20.0 mM (stars). Also Tafel lines at $\phi_2 = 0$ from Anson and Parkinson[5] (dashed line) and from Tyma and Weaver[7] (solid line).

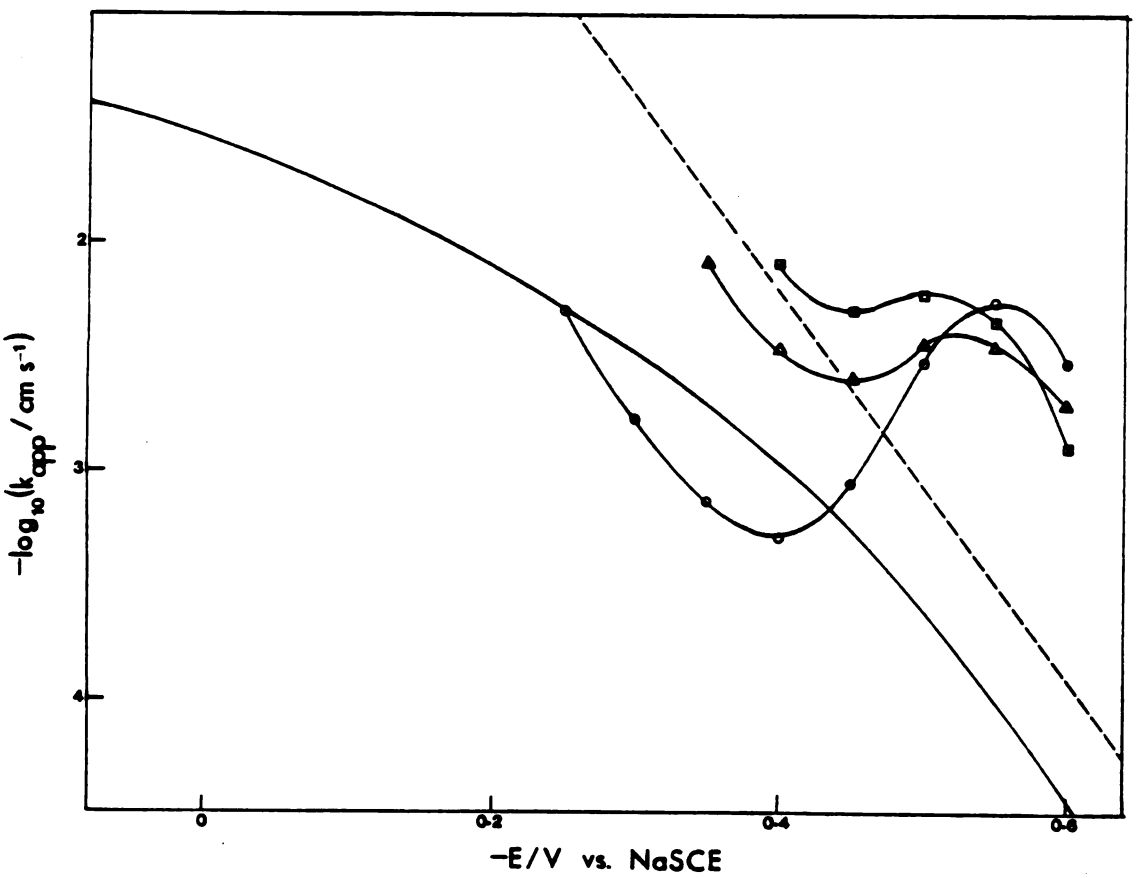

Figure 3.5. Rate-potential for the oxidation of 0.2 mM Eu^{2+} in aqueous solutions of HBr: 0.48 mM (circles); 1.2 mM (triangles); 2.4 mM (squares); Also Tafel lines at $\phi_2 = 0$ from Anson and Parkinson[5] (dashed line) and from Tyma and Weaver[7] (solid line).

Figure 3.6. Double-layer potential (ϕ_2) vs. applied potential (E) curves from the data of Anson and Parkinson[5] for the oxidation of 0.2 mM Eu^{2+} in aqueous solutions of various electrolytes: 1.55 mM $HClO_4$ (circles); 0.8 mM HCl (triangles); 0.48 mM (squares). (ϕ_2 values calculated using Tafel line at ϕ_2 = 0 constructed by Anson and Parkinson[5]).

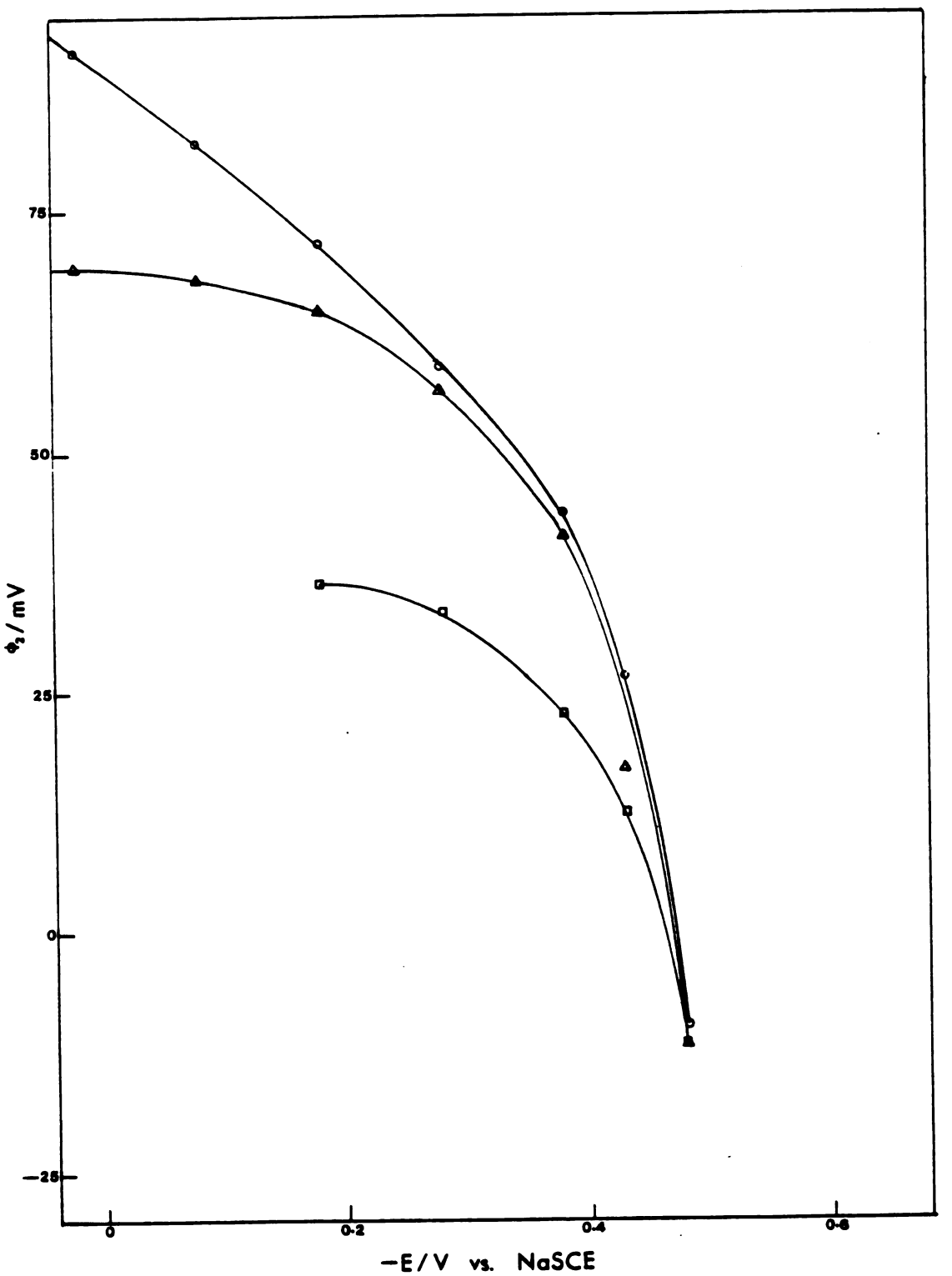

Figure 3.6.

Figure 3.7. Double-layer potential (ϕ_2) vs. applied potential (E) curves from the data of Anson and Parkinson[5] for the oxidation of 0.2 mM Eu^{2+} in aqueous solutions of various electrolytes; 1.55 mM $HClO_4$ (circles); 0.8 mM HCl (triangles); 0.48 mM HBr (squares). (ϕ_2 values calculated using Tafel line at $\phi_2 = 0$ constructed by Tyma and Weaver[7]).

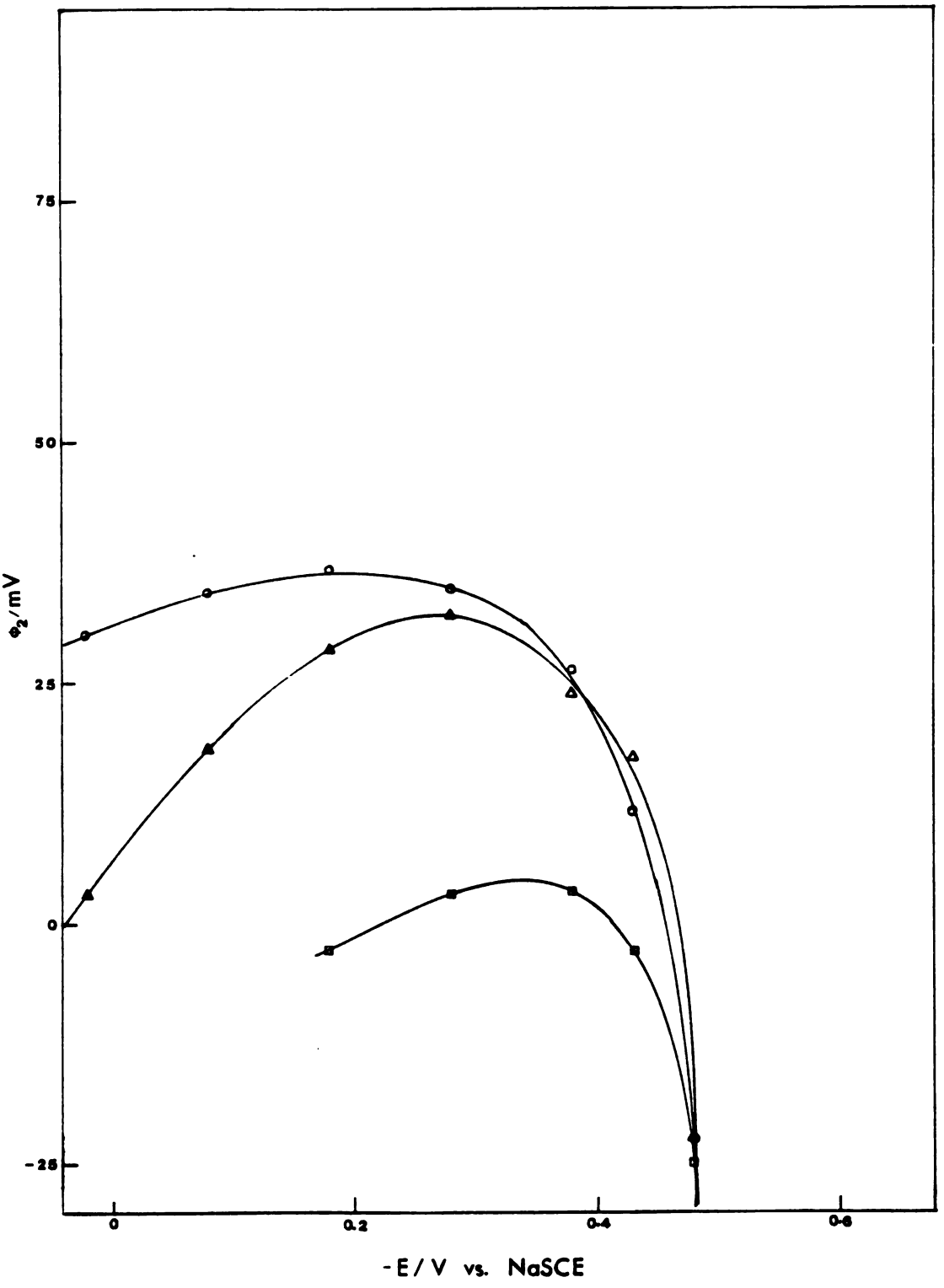

Figure 3.7.

Figure 3.8. Double-layer potential (ϕ_2) vs. applied potential (E) curves for the oxidation of 0.2 m$\underline{M}$ Eu^{2+} in aqueous solutions of various electrolytes: 1.55 m$\underline{M}$ $HClO_4$ (circles); 0.8 m$\underline{M}$ HCl (triangles); 0.48 m$\underline{M}$ HBr (squares). (ϕ_2 values calculated using Tafel line at ϕ_2 = 0 constructed by Anson and Parkinson[5]).

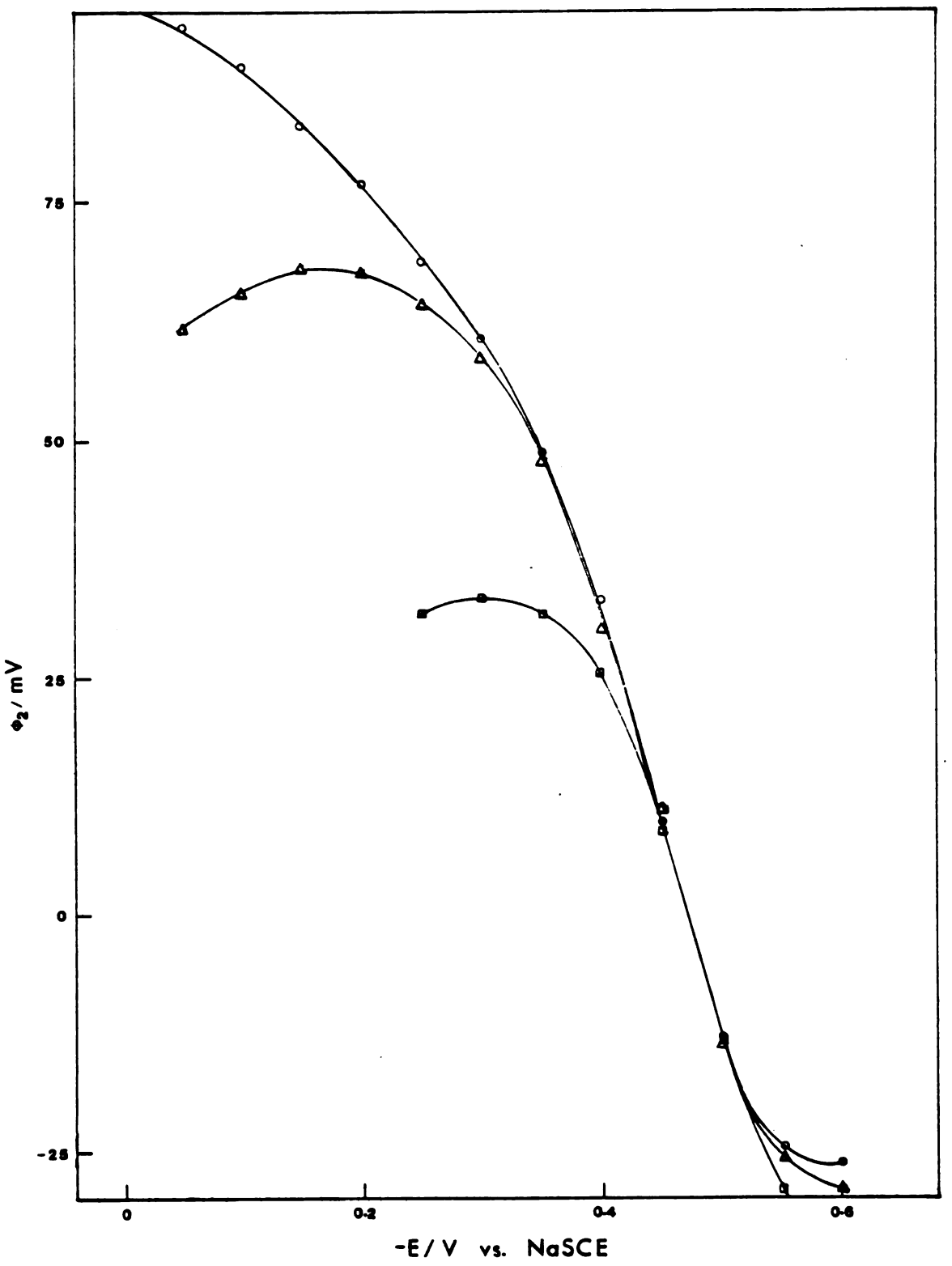

Figure 3.8.

Figure 3.9. Double-layer potential (ϕ_2) vs. applied potential (E) curves for the oxidation of 0.2 mM Eu^{2+} in aqueous solutions of various electrolytes: 1.55 mM $HClO_4$ (circles); 0.8 mM HCl (triangles); 0.48 mM HBr (squares). (ϕ_2 values calculated using Tafel line at ϕ_2 = 0 constructed by Tyma and Weaver[7]).

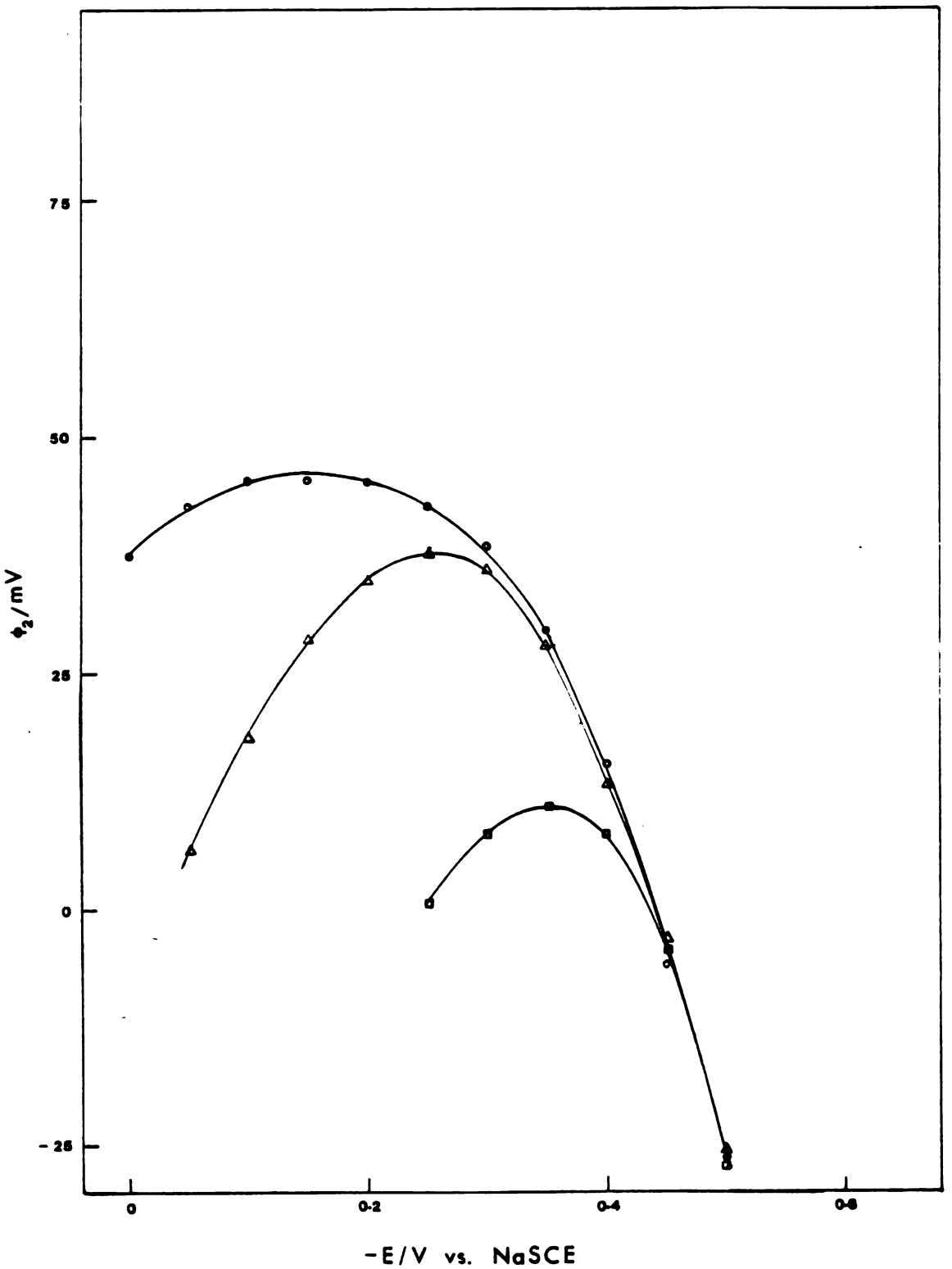

Figure 3.9.

Figure 3.10. Double-layer potential (ϕ_2) vs. applied potential (e) curves for the oxidation of 0.2 m$\underline{M}$ Eu^{2+} in aqueous solutions of $HClO_4$: 1.55 m$\underline{M}$ (circles); 4.0 m$\underline{M}$ (triangles); 7.75 m$\underline{M}$ (squares). (ϕ_2 values calculated using Tafel line at $\phi_2 = 0$ constructed by Anson and Parkinson[5]).

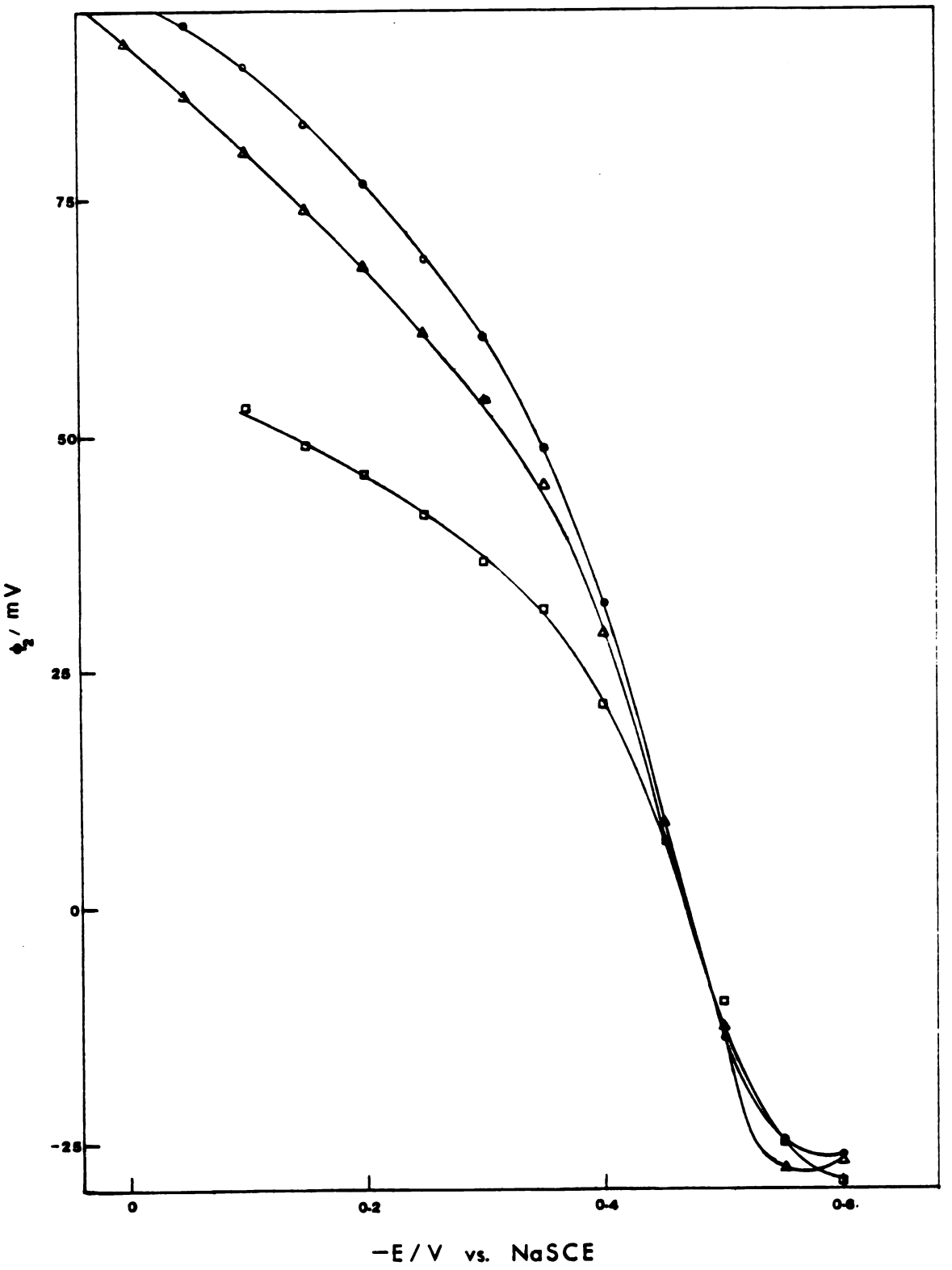

Figure 3.10.

Figure 3.11. Double-layer potential (ϕ_2) vs. applied potential (E) curves for the oxidation of 0.2 mM Eu^{2+} in aqueous solutions of $HClO_4$: 1.55 mM (circles); 4.0 mM (triangles); 7.75 mM (squares). (ϕ_2 values calculated using Tafel line at $\phi_2 = 0$ constructed by Tyma and Weaver[7]).

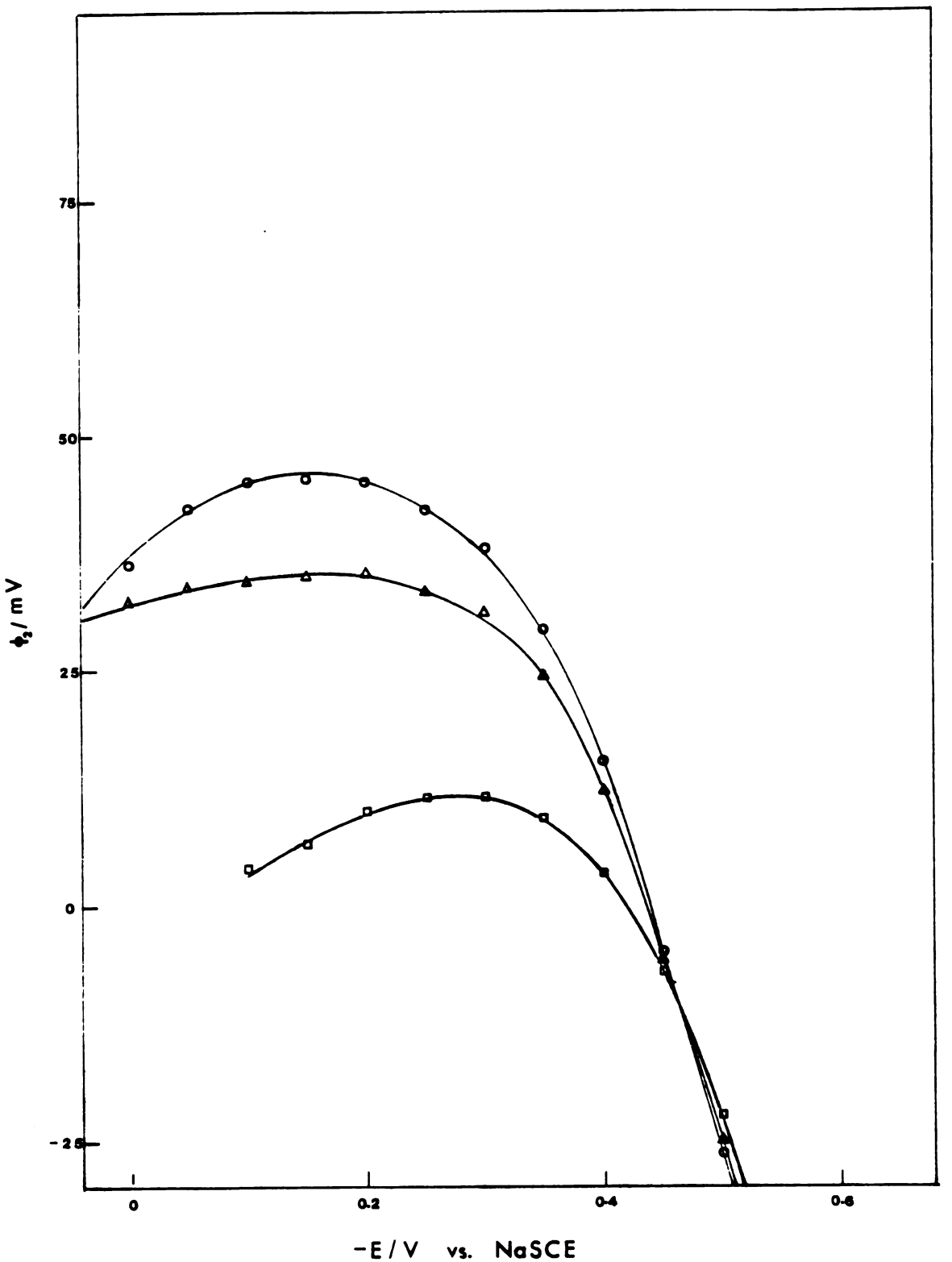

Figure 3.11.

Figure 3.12. Double-layer potential (ϕ_2) vs. applied potential (E) curves for the oxidation of 0.2 mM Eu^{2+} in aqueous solutions of HCl: 0.8 mM (circles); 2.0 mM (triangles); 4.0 mM (squares); 20.0 mM (stars). (ϕ_2 values calculated using Tafel line at $\phi_2 = 0$ constructed by Anson and Parkinson[5]).

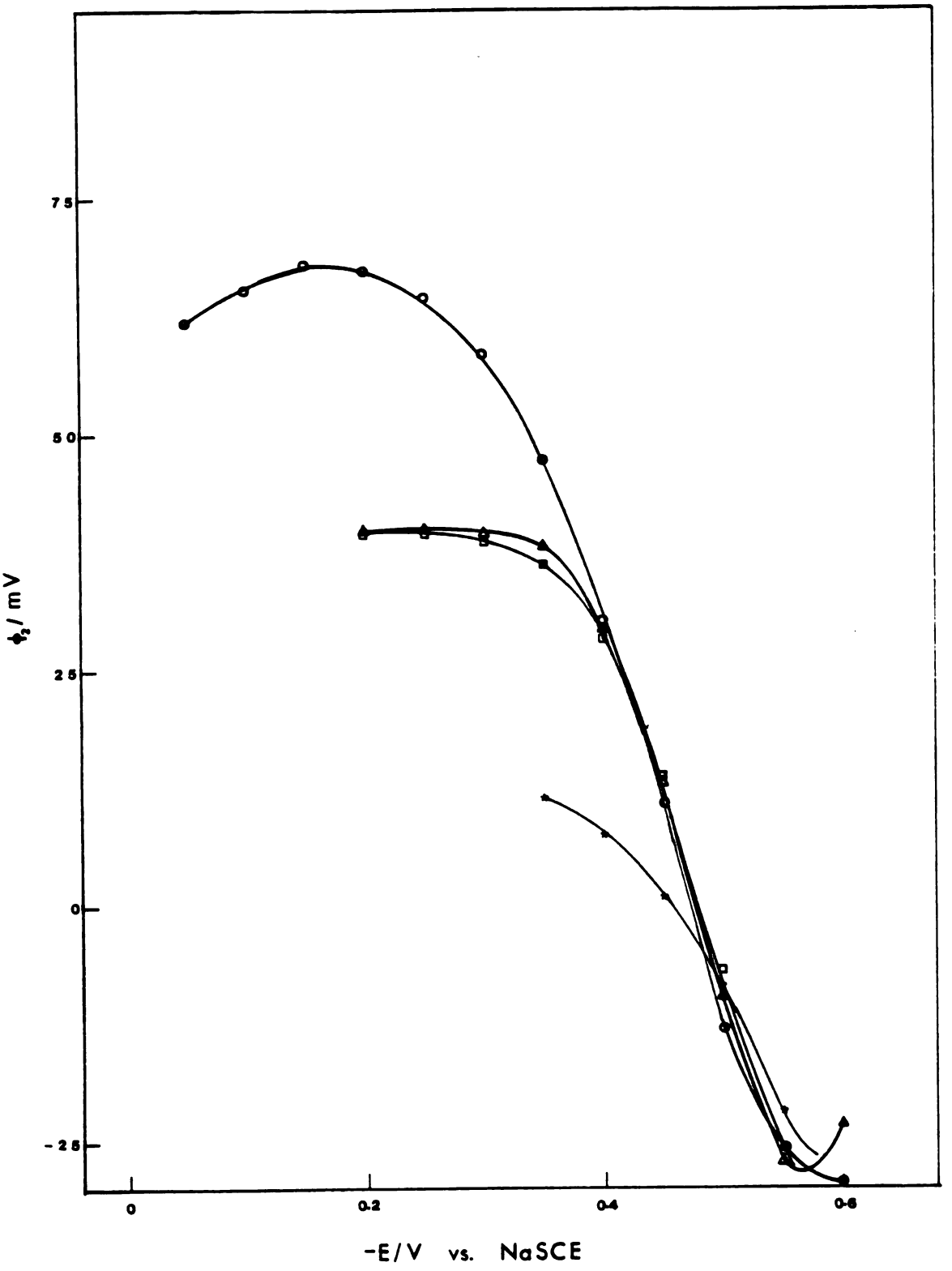

Figure 3.12.

Figure 3.13. Double-layer potential (ϕ_2) vs. applied potential (E) curves for the oxidation of 0.2 mM Eu^{2+} in aqueous solutions of HCl: 0.8 mM (circles); 2.0 mM (triangles); 4.0 mM (squares); 20.0 mM (stars). (ϕ_2 values calculated using Tafel line at ϕ_2 = 0 constructed by Tyma and Weaver[7]).

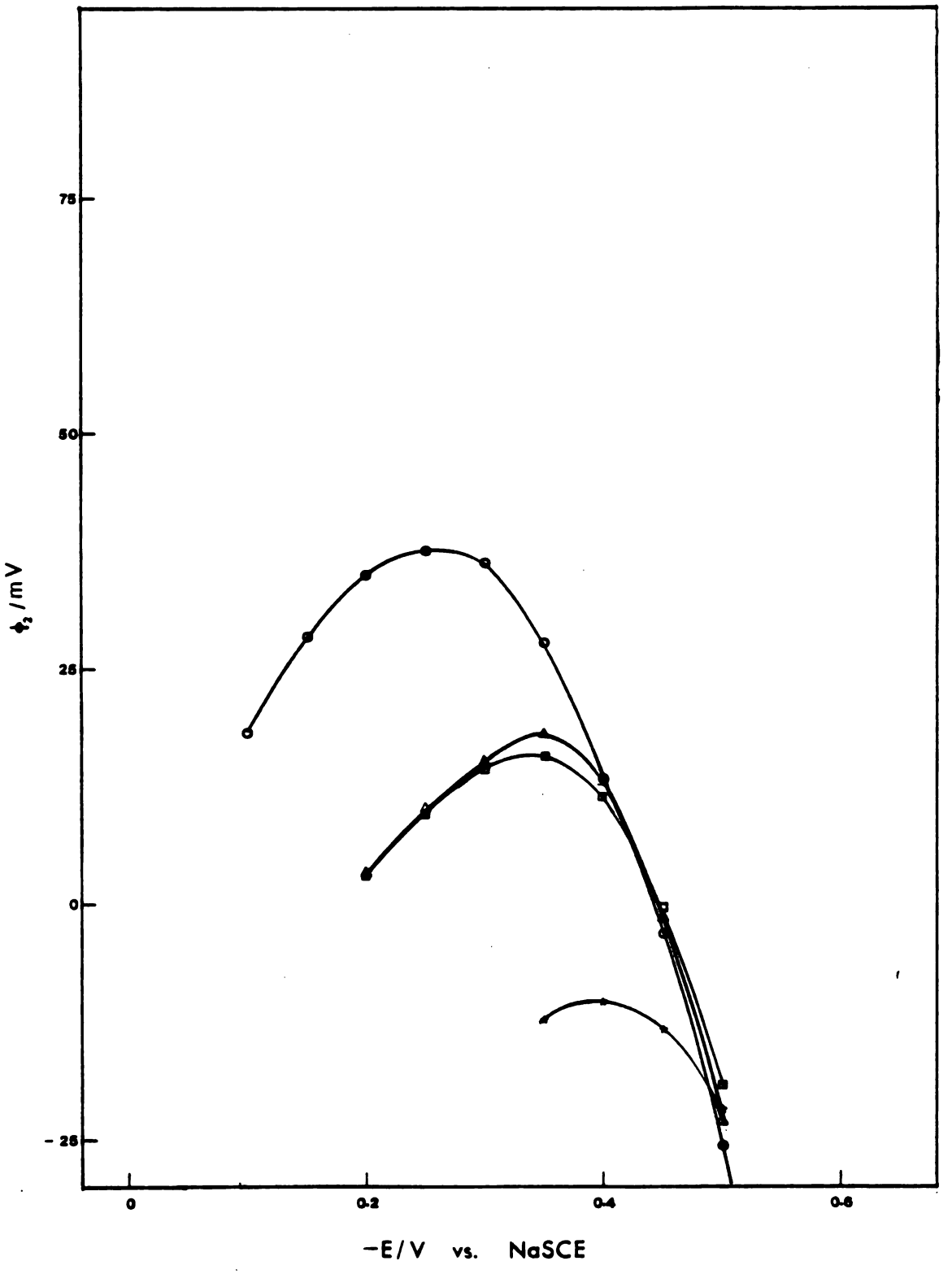

Figure 3.13.

Figure 3.14. Double-layer potential (ϕ_2) vs. applied potential (E) curves for the oxidation of 0.2 mM Eu^{2+} in aqueous solutions of HBr: 0.48 mM (circles); 1.2 mM (triangles); 2.4 mM (squares). ($\bar{\phi}_2$ values calculated using Tafel line at $\phi_2 = 0$ constructed by Anson and Parkinson[5]).

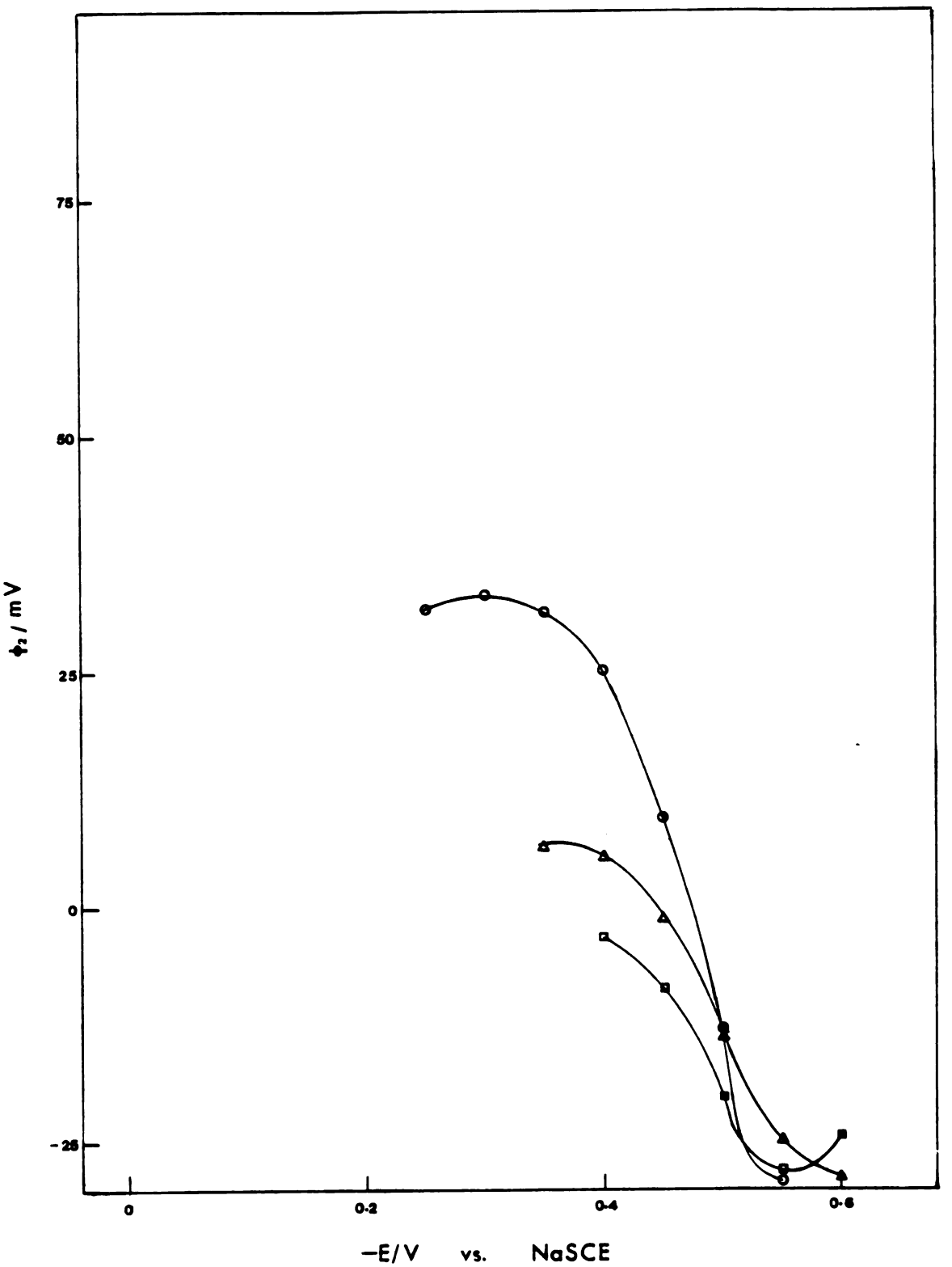

Figure 3.14.

Figure 3.15. Double-layer potential (ϕ_2) vs. applied potential (E) curves for the oxidation of 0.2 mM Eu^{2+} in aqueous solutions of HBr: 0.48 mM (circles); 1.2 mM (triangles); 2.4 mM (squares). (ϕ_2 values calculated using Tafel line at $\phi_2 = 0$ constructed by Tyma and Weaver[7]).

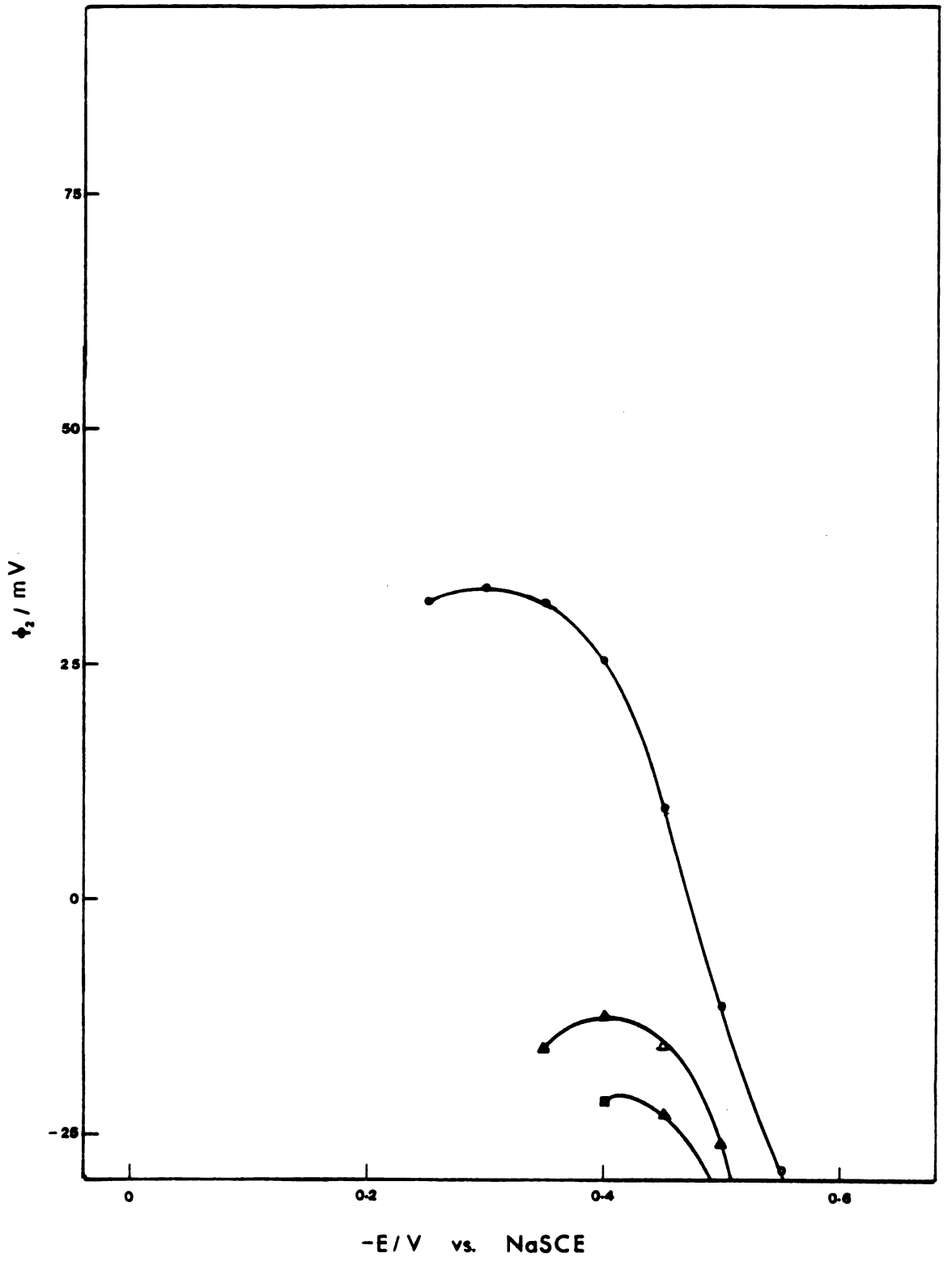

Figure 3.15.

Figure 3.16. Charge-potential curves (from the data of Anson and Parkinson[5]) for the oxidation of 0.2 m$\underline{M}$ Eu^{2+} in aqueous solutions of various electrolytes calculated from GCS model using ϕ_2 values from Figure 3.6: 1.55 m$\underline{M}$ $HClO_4$ (circles); 0.8 m$\underline{M}$ HCl (triangles); 0.48 m$\underline{M}$ HBr (squares).

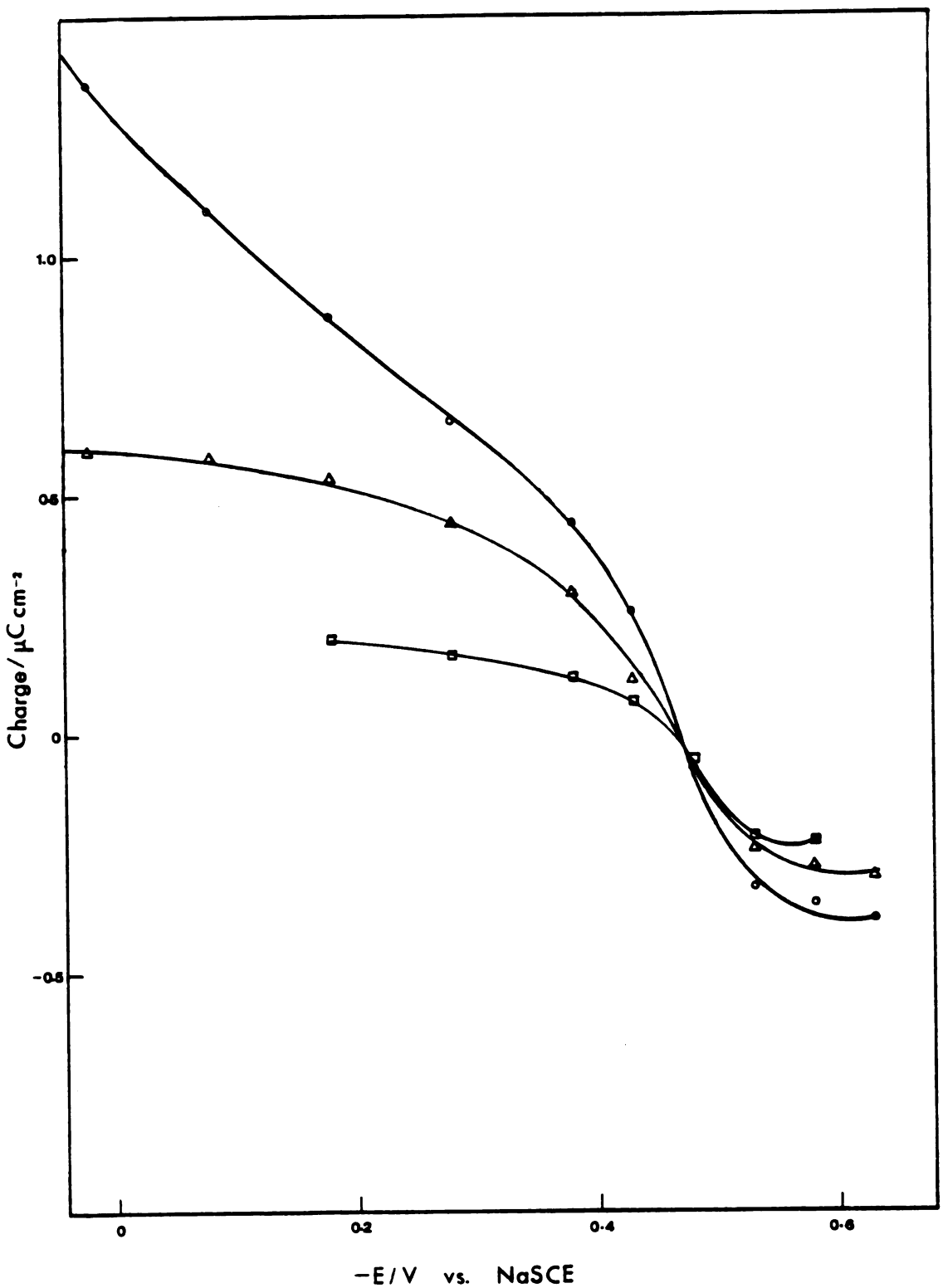

Figure 3.16.

Figure 3.17. Charge-potential curves (from the data of Anson and Parkinson[5]) for the oxidation of 0.2 m$\underline{M}$ Eu^{2+} in aqueous solutions of various electrolytes calculated from GCS model using ϕ_2 from Figure 3.7: 1.55 m$\underline{M}$ $HClO_4$ (circles); 0.8 m$\underline{M}$ HCl (triangles); 0.48 m$\underline{M}$ HBr (squares).

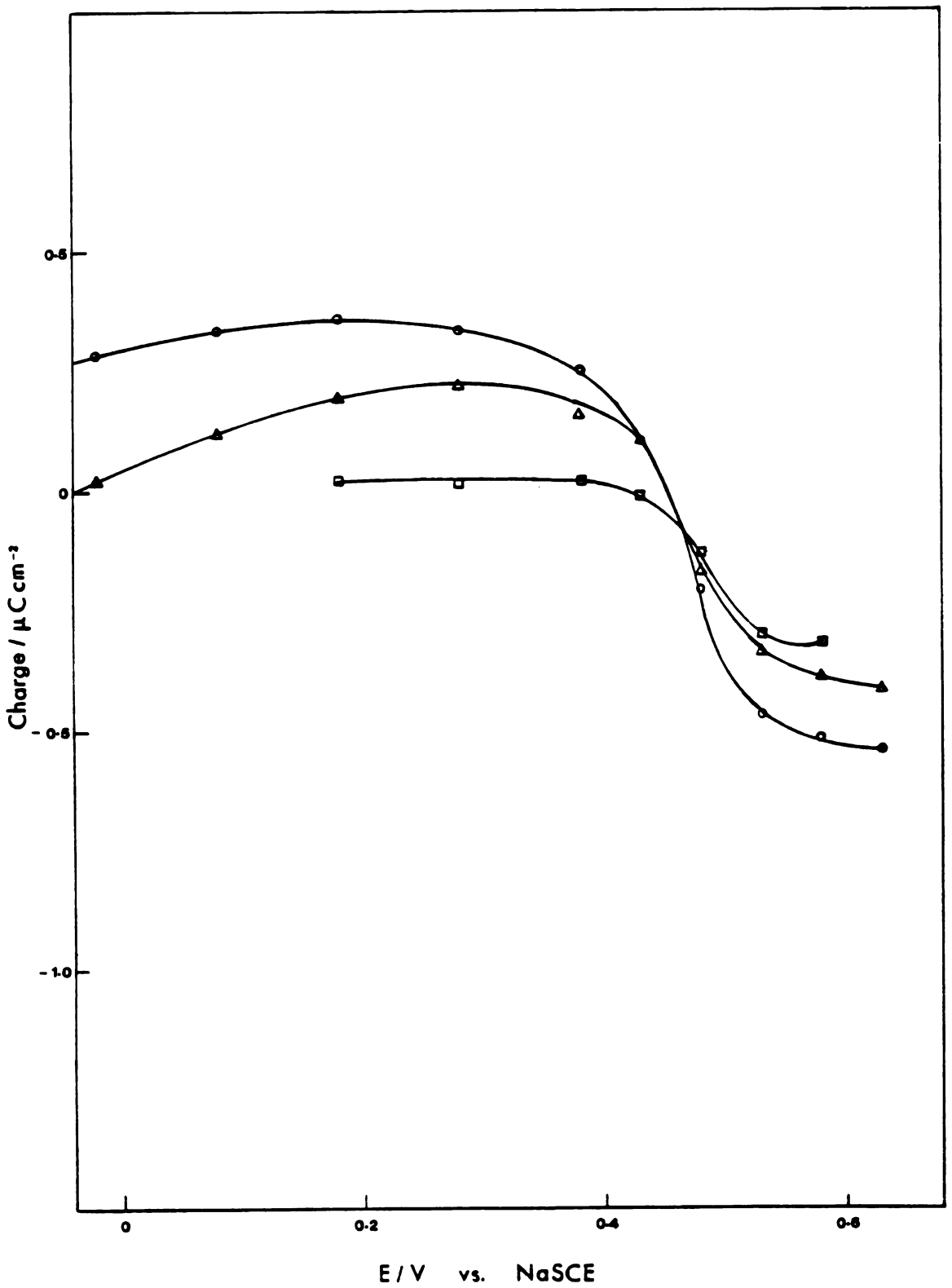

Figure 3.17.

Figure 3.18. Charge-potential curves for the oxidation of 0.2 mM Eu^{2+} in aqueous solutions of various electrolytes calculated from GCS model using ϕ_2 values from Figure 3.8: 1.55 mM $HClO_4$ (circles); 0.8 mM HCl (triangles); 0.48 mM HBr (squares).

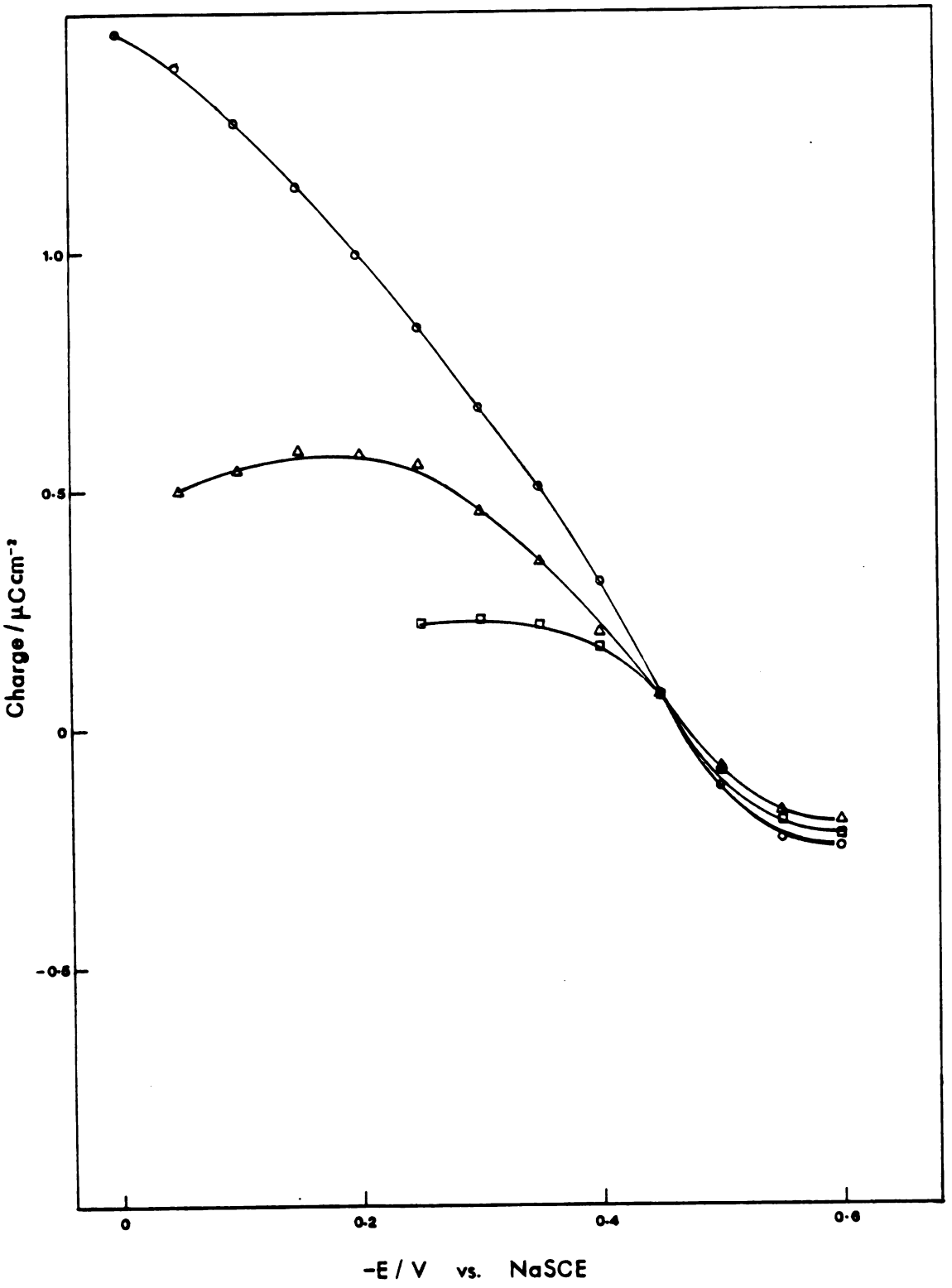

Figure 3.18.

Figure 3.19. Charge-potential curves for the oxidation of 0.2 mM Eu^{2+} in aqueous solutions of various electrolytes calculated from GCS model using ϕ_2 values from Figure 3.9: 1.55 mM $HClO_4$ (circles); 0.8 mM HCl (triangles); 0.48 mM HBr (squares).

oxidation
ions of
from GCS
re 3.9:
HCl
es).

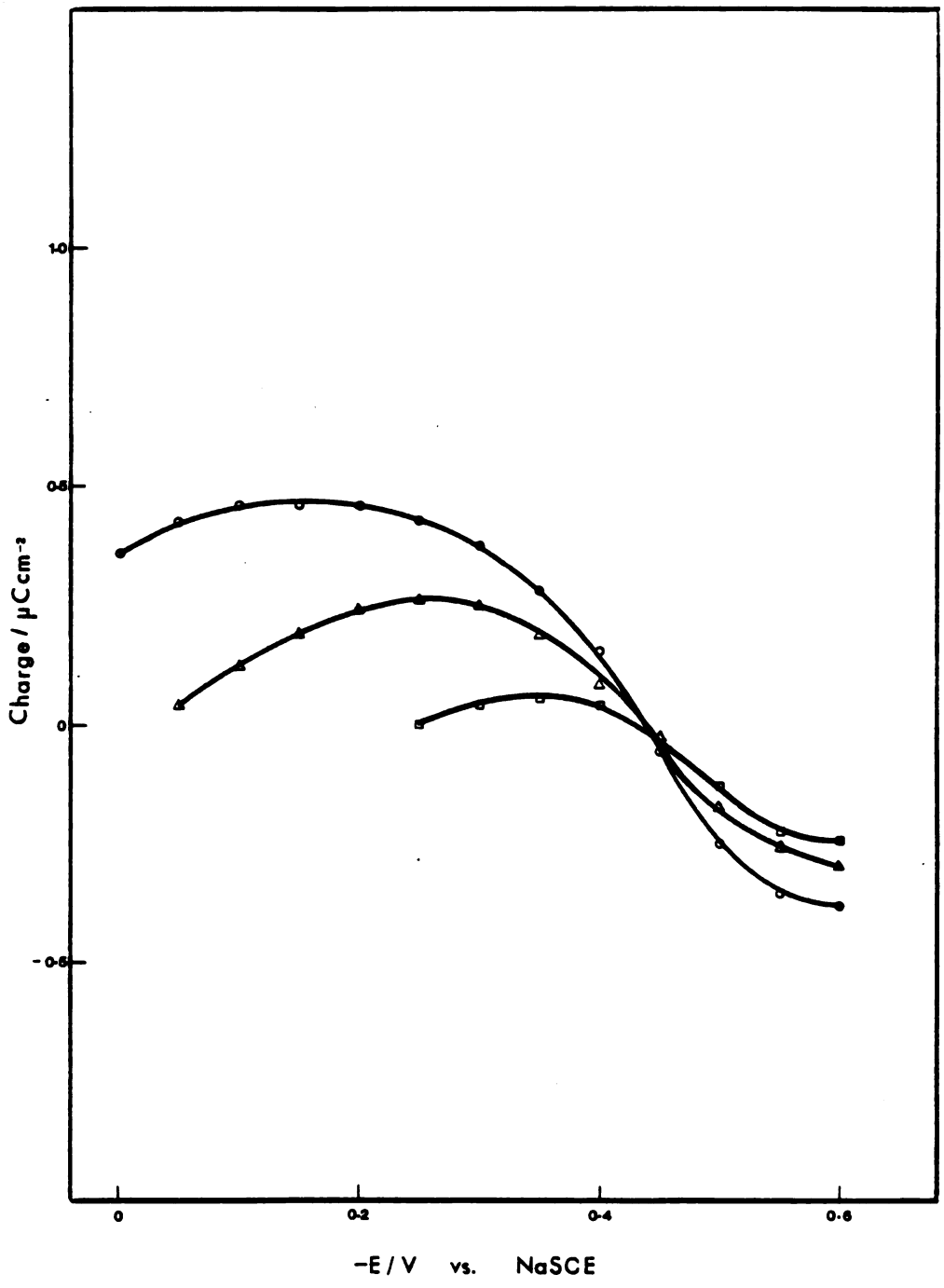

Figure 3.19.

Figure 3.20. Charge-potential curves for the oxidation of 0.2 mM Eu^{2+} in aqueous solutions of $HClO_4$ calculated from GCS model using ϕ_2 values from Figure 3.10; 1.55 mM (circles); 4.0 mM (triangles): 7.75 mM (squares).

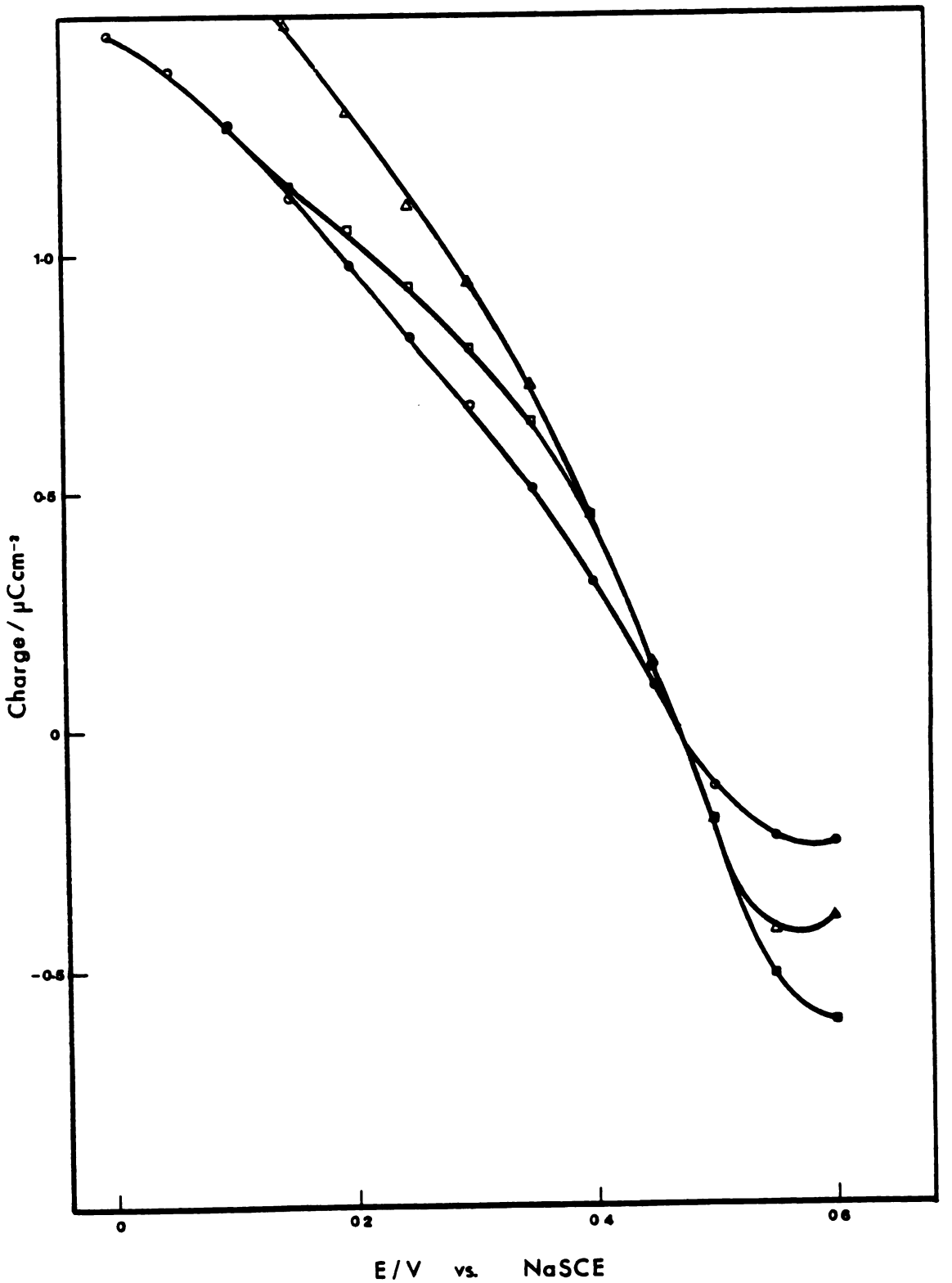

Figure 3.20.

Figure 3.21. Charge-potential curves for the oxidation of 0.2 m$\underline{M}$ Eu^{2+} in aqueous solutions of $HClO_4$ calculated from GSC model using ϕ_2 values from Figure 3.11, 1.55 m$\underline{M}$ (circles); 4.0 m$\underline{M}$ (triangles); 7.75 m$\underline{M}$ (squares).

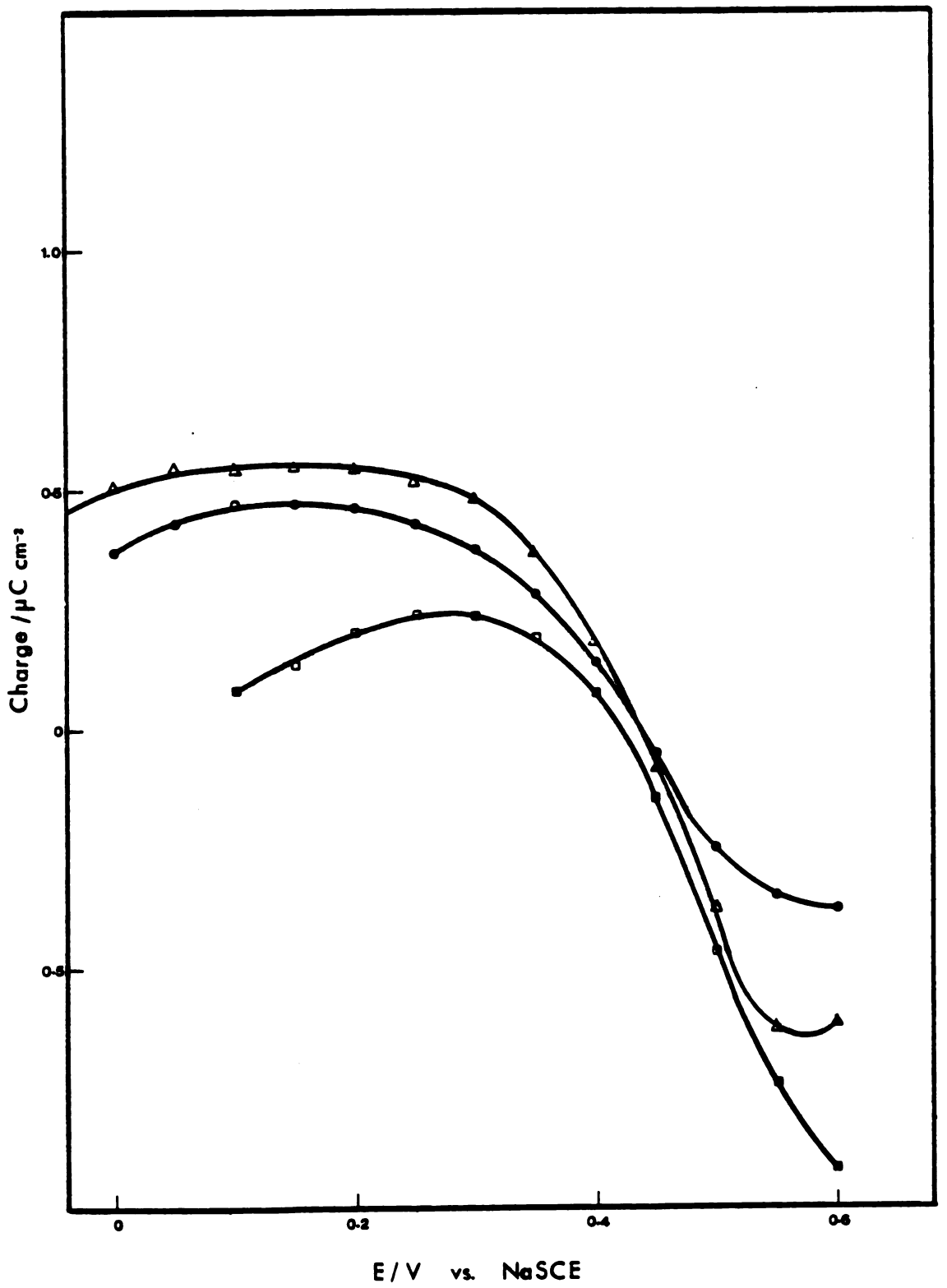

Figure 3.21.

Figure 3.22. Charge-potential curves for the oxidation of 0.2 m$\underline{M}$ Eu^{2+} in aqueous solutions of HCl calculated from GCS model using ϕ_2 values from Figure 3.12: 0.8 m$\underline{M}$ (circles); 2.0 m$\underline{M}$ (triangles); 4.0 m$\underline{M}$ (squares); 20.0 m$\underline{M}$ (stars).

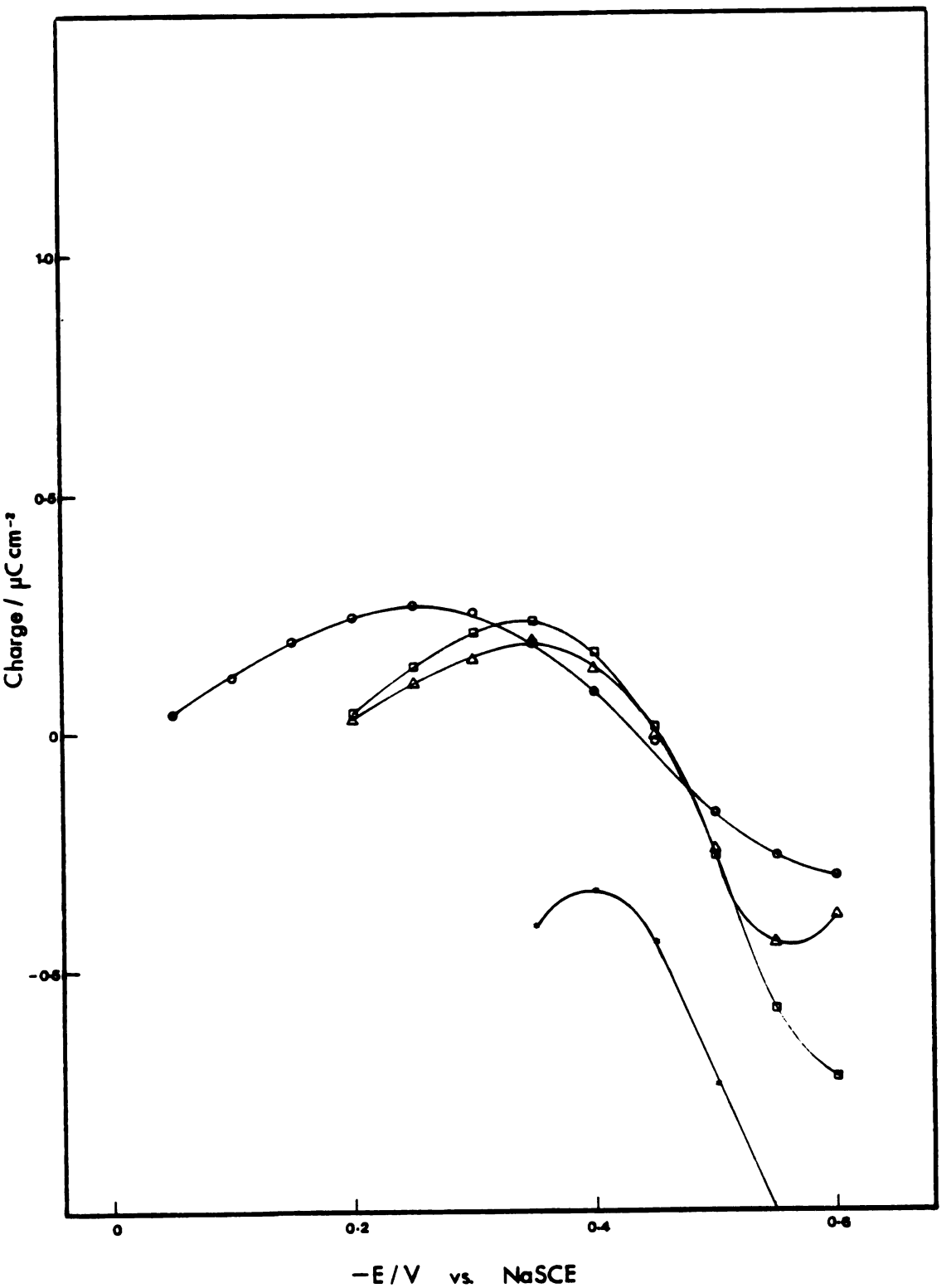

Figure 3.22.

Figure 3.23. Charge-potential curves for the oxidation of 0.2 mM Eu^{2+} in aqueous solutions of HCl calculated from GCS model using ϕ_2 values from Figure 3.13: 0.8 mM (circles); 2.0 mM (triangles); 4.0 mM (squares); 20.0 mM (stars).

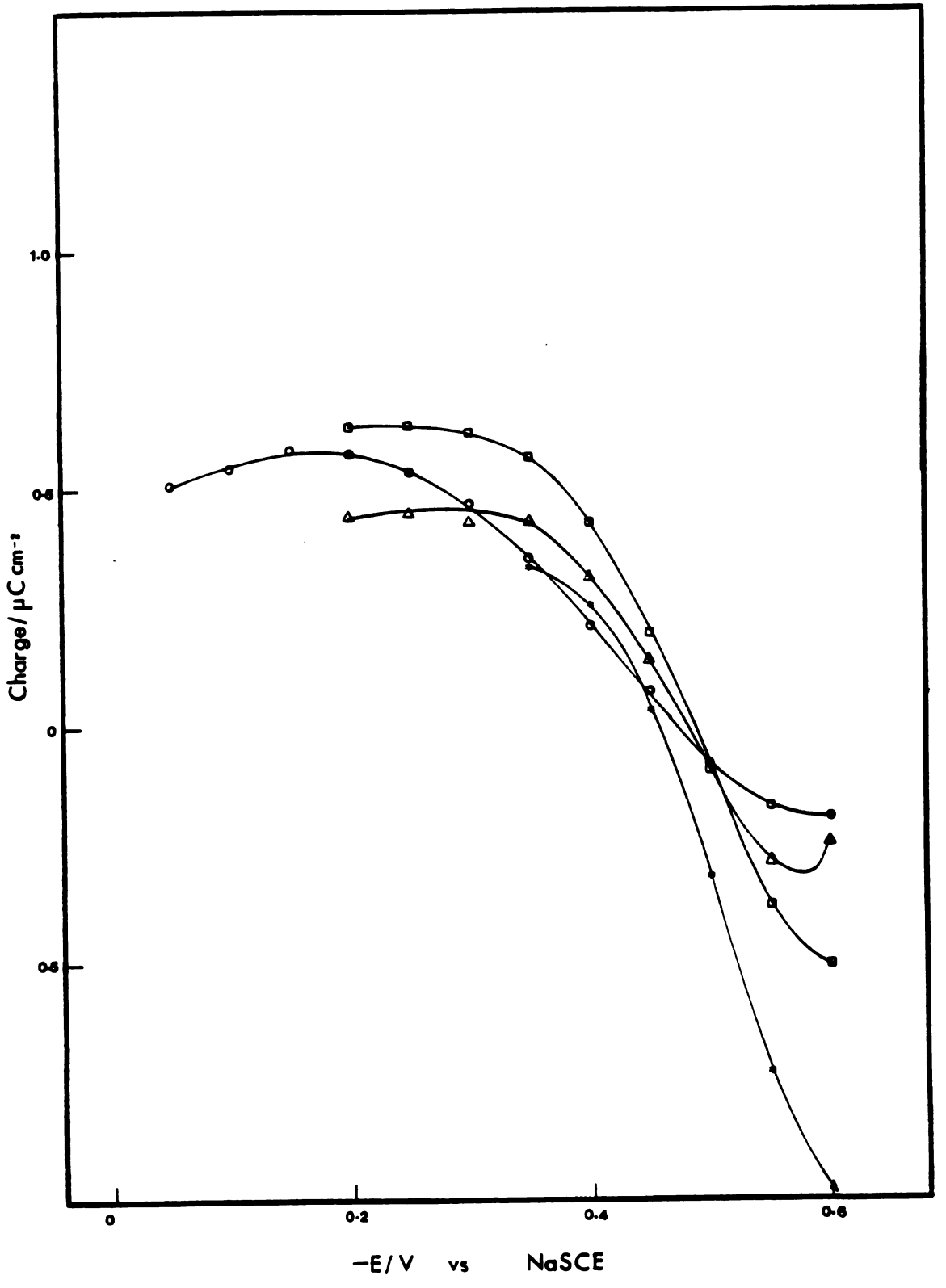

Figure 3.23.

Figure 3.24. Charge-potential curves for the oxidation of 0.2 m$\underline{M}$ Eu^{2+} in aqueous solution of HBr calculated from GCS model using ϕ_2 values from Figure 3.14: 0.48 m$\underline{M}$ (circles); 1.2 m$\underline{M}$ (triangles); 2.4 m$\underline{M}$ (squares).

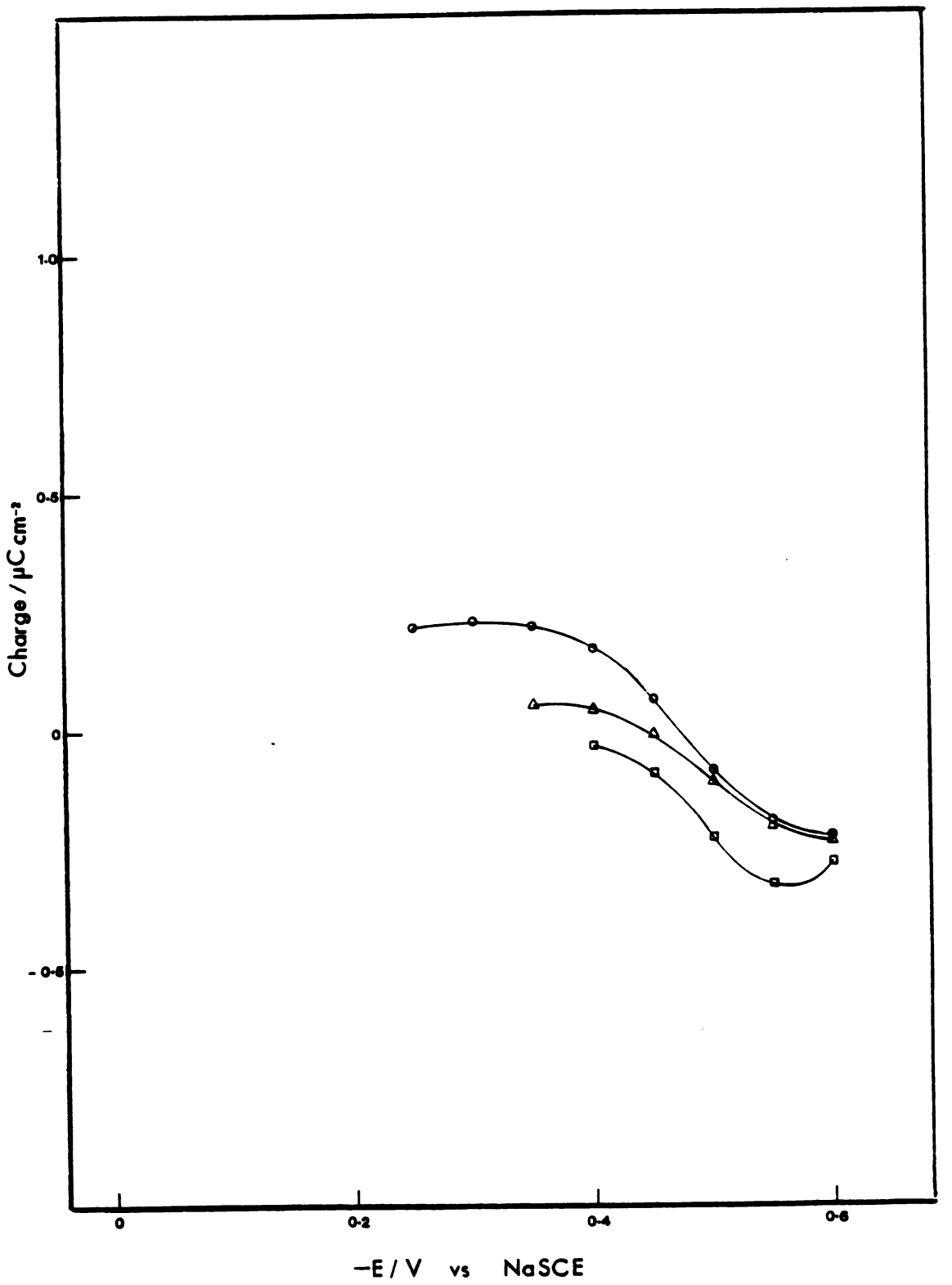

Figure 3.24.

Figure 3.25. Charge-potential curves for the oxidation of 0.2 m$\underline{M}$ Eu^{2+} in aqueous solutions of HBr calculated from GCS model using ϕ_2 values from Figure 3.15: 0.48 m$\underline{M}$ (circles); 1.2 m$\underline{M}$ (triangles); 2.4 m$\underline{M}$ (squares).

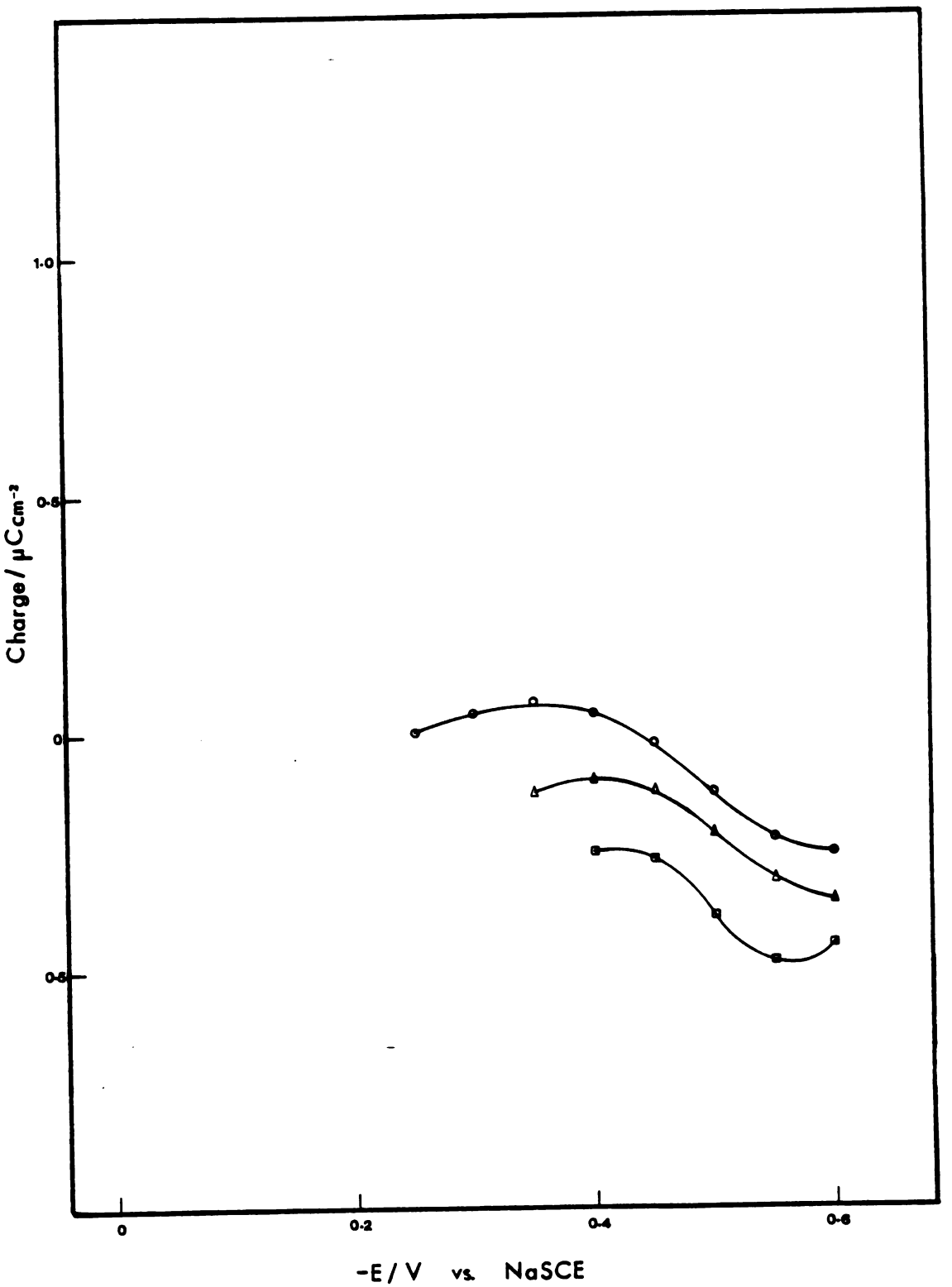

Figure 3.25.

study for the measurement of ϕ_{rp} from the kinetic data are based on the replacement of Tafel line at $\phi_2 = 0$, constructed by Anson and Parkinson[5], with the assumption that α is constant throughout the potential range, with a more realistic Tafel line at $\phi_2 = 0$ constructed by Tyma and Weaver[7]. The use of the correct Tafel line[7] essentially reduces the magnitude of the ϕ_2 values in comparison with the experimental results of Anson and Parkinson[5] and brings them within the range of experimental uncertainty for the static method (electrocapillary data), obtained by Anson and Parkinson[5].

The static method was carried out by obtaining charge-potential curves for the solution of electrolyte before and after adding multiple charged ions which are electrochemically unreactive in the potential range of interest such as $Cr(CN)_6^{3-}$ in dilute $HClO_4$ solution. Any shift in the curve would be attributed to the preferential attraction of the multiply charged anion into the anionic diffuse layer. With $HClO_4$ electrolyte, the small changes in q^m with the addition of $Cr(CN)_6^{3-}$ were interpreted to show that the potential differences across the diffuse layer is negligibly small, and hence, the inference was made that the diffuse layer is absent in dilute solution. The experimental precision with which charge-potential curves were measured was not high enough to distinguish between the complete absence of a diffuse layer and the presence of a diffuse layer containing

a few tenths $\mu C cm^{-2}$ of ionic charge. Therefore, even though it is within the range of experimental uncertainty, it may be assumed that the diffuse layer is still present in dilute solutions of electrolytes.

CHAPTER IV

THE pH DEPENDENCE OF ELECTROCHEMICAL RATE CONSTANTS OF TRANSITION METAL AQUO COMPLEXES IN AQUEOUS SOLUTION

A. A number of papers on heterogeneous electrochemical reaction kinetics refer to the very simple redox kinetics of the aquo-complexes of first transition metal series in aqueous solution and the authors assume that the simplicity provides a dependable basis for comparing their results with similar kinetic observations. In most cases, the results for the heterogeneous kinetic rate constants for these systems were left unchecked for dependence on the pH of the working solution. It is generally assumed that the working bounds for the electrochemical reaction of these systems are based upon only two major factors:

a) The precipitation out or formation of dissolved hydroxides of the metals at high pH values.
b) The potential for the hydrogen evolution reaction at the electrode at very low pH values.

The heterogeneous kinetics were assumed to remain unaffected by the variation of pH between those two bounds. The kineticists, hence, took the liberty of working with these systems at their choices of pH values and comparing

the results even for different pH values.

A puzzling situation arose with the $V_{aq}^{3+/2+}$ couple for which the rates of the reaction are not independent of the pH of the solution. This situation was further elaborated by performing experiments at constant ionic strength while varying the amounts of $HClO_4$ and $LiClO_4$ in the solution. The ionic strength was kept constant to make sure that other effects, for example, the double-layer structure do not vary at different pH values.

After it was found that behavior of the $V_{aq}^{3+/2+}$ couple is dependent on pH, similar couples from the first transition series were checked for the same and it was found that only $V_{aq}^{3+/2+}$ couple has pH dependent behavior.

B. Experimental procedure and analysis of data

Solutions of 1 m$\underline{M}$, V^{2+}, Cr^{2+}, Mn^{2+}, Fe^{2+}, Co^{2+}, Ni^{2+}, Zn^{2+} and Eu^{2+} ion in different concentrations of supporting electrolytes were prepared in 0.02 $\underline{M}$, 0.10 $\underline{M}$ and 0.40 $\underline{M}$ $HClO_4$ by adding enough $LiClO_4$ to make the ionic concentration 1 $\underline{M}$ for all solutions. Cyclic voltammetric measurements were made for reversible or quasi-reversible redox reactions for the aquo complexes of $V^{3+/2+}$ and $Zn^{2+/0}$ couples, while for the other couples of the aquo complexes of $Eu^{3+/2+}$, $Cr^{3+/2+}$, $Mn^{2+/0}$, $Fe^{3+/2+}$, $Co^{2+/0}$, $Ni^{2+/0}$ and $Fe^{2+/0}$ dc polarography was employed for the reduction reaction. The pH of the solutions was measured before

and after the electrochemical experiments. The results from cyclic voltammetry were analyzed using the method outlined by Nicholson[16] while dc polarographic results were analyzed using the Koutecky[13, 14] method. The k_{net} was plotted against $1/[H^+]$ for V^{2+} since it was the only system showing the pH dependence.

C. Results and Discussion

When a metal ion is dissolved in water, it is well established that it interacts strongly with water molecules, and these water molecules are bound to the metal ions via the oxygen atom to form strong coordinate linkages by virtue of the electron lone pairs. In the strict sense, therefore, it is meaningless to speak of "simple" metal ions in solution since the actual state of such species is that of an aquo-complex in which water molecules are to be regarded as ligands. The bond between O and H in the coordinated water molecule depends upon the acidity of the central metal ion. In cases of high acidity of the central metal cation, it can cause rupture of the O-H bonds resulting in the hydrolysis of the metal aquo complex and leaving the complex with -OH ligands.

$$M^{n+} + x\ H_2O \rightarrow [M(H_2O)_m^{n+}] \rightleftharpoons H^+ [M(H_2O)_{m-1}OH]^{(n-1)+} \quad (4.1)$$

The formation of the hydroxyl complex, hence, changes the homogeneous and heterogeneous kinetics of the redox reactions. It implies from equation 4.1 that a pH range

can be defined for the stability of these complexes which depends upon the hydrolysis constant K_h for the species [3, 4, 50]. Another effect which may arise here is that the formal potential for the $M(H_2O)_m^{n+}$ / $M[(OH_x(H_2O)_{m-x}]^{(n-x)+}$ couple, which depends mainly upon the pH of the solution, may lie close to the formal potentials for $M(H_2O)_m^{n+}$ / $M(H_2O)_m^{(n-1)+}$ or $[M(OH)_x(H_2O)_{m-x}]^{(n-x)+}$ / $[M(OH_{x-1}(H_2O)_{m-x+1}^{(n-x+1)+}]$ couples, making the kinetic study of the aquocation complexes more complicated, because these reactions contribute to the overall rate of the reaction in a way that depends on the pH of the solution. The equilibrium constant for the hydrolysis reaction (K_h) along with the formal potentials for the redox couples including the hydroxo complexes can be used to give a workable range of pH to study just the redox kinetics of aquo complexes.

The related values for the hydrolysis of the redox couples under study (Table 4.1) clearly indicate that all systems except $V_{aq}^{3+/2+}$ and $Fe_{aq}^{3+/2+}$ have a relatively broad working range of pH when the hydrolysis does not occur. The simple hydrolysis reactions for the aquo complexes of V^{2+} and V^{3+} behave in a similar fashion to the Fe_{aq}^{2+}, Fe_{aq}^{3+} complexes, i.e., that is a larger working pH range for V^{2+} and a very narrow range for V^{3+}. The situation however, is more complicated than Fe^{3+} and Fe^{2+} since both V^{3+} and V^{2+} ions have relatively larger capacity to form a variety of hydroxo compounds and polymers at low pH values [55-58].

Table 4.1. Related values for the hydrolysis constant for some redox couples.

Metal Ion	Reaction	Related Information	Reference
1. Eu^{2+}	$Eu^{3+} + e^- \leftrightharpoons Eu^{2+}$	$E_o = -0.429 + 0.0591 \log\frac{[Eu^{3+}]}{[Eu^{2+}]}$	(55)
2. Eu^{3+}	$Eu^{3+} + 3H_20 \leftrightharpoons Eu(OH)_3 + 3H^+$	$\log\frac{[Eu(OH)_3]}{[Eu^{3+}]} = -21.5 + 3pH$	(56,57)
3. V^{2+}	$V^{3+} + e^- \leftrightharpoons V^{2+}$	$E_o = -0.255 + 0.0591 \log\frac{[V^{3+}]}{[V^{2+}]}$	(55)
	$V^{2+} + H_20 \leftrightharpoons VOH^+ + H^+$	$\log\frac{[VOH^+]}{[V^{2+}]} = pH - 6.49$, evidence of V_20^{2+} predominant at 0.1M H^+ and 0.2M $NAClO_4$.	(56)
	$V^{2+} + H_20 \leftrightharpoons VOH^{2+} + H^+ + e-$	$E_o = -0.082 - 0.0591pH + 0.0591 \log\frac{[VOH^{2+}]}{[V^{2+}]}$	(55)
	$V^{2+} + H_20 \leftrightharpoons VO^+ + 2H^+ + e-$	$E_o = 0.126 - 0.1182pH + 0.0591 \log\frac{[VO^+]}{[V^{2+}]}$	(55)

Table 4.1 (cont'd.)

Metal Ion	Reaction	Related Information	Reference
4. V^{3+}	$V^{3+} + H_2O \rightleftharpoons VOH^{2+} + H^+$	$\log\frac{[VOH^{2+}]}{[V^{3+}]} = pH - 2.92$	
		evidence of $V_2(OH)_2^{2+}$ in 1M $LiClO_4$, $V_2(OH)_3^{3+}$, $V_3(OH)_4^{5+}$ and other larger polymers.	(55,56,57,58)
	$VOH^{2+} \rightleftharpoons VO^+ + H^+$	$\log\frac{[VO^+]}{[VOH^{2+}]} = pH - 3.52$	(55,56,57)
5. Cr^{2+}	$Cr^{3+} + e^- \rightleftharpoons Cr^{2+}$	$E_o = -0.407 + 0.0591 \log\frac{[Cr^{3+}]}{[Cr^{2+}]}$	(55)
	$Cr^{2+} + H_2O \rightleftharpoons CrOH^+ + H^+$	$\log\frac{[Cr(OH)_2]}{[Cr^{2+}]} = 2pH - 11$	(56)
	$Cr^{2+} + H_2O \rightleftharpoons CrOH^{2+} + H^+ + e^-$	$E_o = -0.182 - 0.0591pH + 0.0591 \log\frac{[CrOH^{2+}]}{[Cr^{2+}]}$	(55)

Table 4.1 (cont'd.)

Metal Ion	Reaction	Related Information	Reference
6. Cr^{3+}	$Cr^{3+} + H_2O \rightleftharpoons CrOH^{2+} + H^+$	$\log\frac{[CrOH^{2+}]}{[Cr^{3+}]} = pH - 4.1$	(55,56,57)
	$CrOH^{2+} + H_2O \rightleftharpoons Cr(OH)_2^+ + H^+$	$\log\frac{[Cr(OH)_2^+]}{[CrOH^{2+}]} = pH - 6.22$	(55,56,57)
7. Mn^{2+}	$Mn^{2+} + H_2O \rightleftharpoons MnOH^+ + H^+$	$\log\frac{[MnOH^+]}{[Mn^{2+}]} = pH - 10.5$	(55,56)
	$Mn^{2+} + 2H_2O \rightleftharpoons HMnO_2^- + 3H^+$	$\log\frac{[HMnO_2^-]}{[Mn^{2+}]} = 2pH - 34.39$	(55,56)
8. Fe^{2+}	$Fe^{3+} + e^- \rightleftharpoons Fe^{2+}$	$E_o = 0.771 + 0.0591 \log\frac{[Fe^{3+}]}{[Fe^{2+}]}$	(55)
	$Fe^{2+} + H_2O \rightleftharpoons FeOH^+ + H^+$	$\log\frac{[FeOH^+]}{[Fe^{2+}]} = pH - 8.3$	(55,56,57)
	$Fe^{2+} + H_2O \rightleftharpoons FeOH^{2+} + H^+ + e^-$	$E_o = 0.914 - 0.0591\ pH + 0.0591 \log\frac{[FeOH^{2+}]}{[Fe^{2+}]}$	(55)

Table 4.1 (cont'd.)

Metal Ion	Reaction	Related Information	Reference
	$Fe(OH)_2 \rightleftharpoons Fe^{2+} + 2OH^-$	$\log\frac{[Fe(OH)_2]}{[Fe^{2+}]} = 2pH - 12.9$	(55,56,57)
9. Fe^{3+}	$Fe^{3+} + H_2O \rightleftharpoons FeOH^{2+} + H^+$	$\log\frac{[FeOH^{2+}]}{[Fe^{3+}]} = pH - 2.46$	(55,56,57)
	$Fe(OH)_3 \rightleftharpoons Fe^{3+} + 3OH^-$	$\log\frac{[Fe^{3+}]}{[Fe(OH)_3]} = 2.96 - 3pH$	(55,56,57)
10. Co^{2+}	$Co^{3+} + e^- \rightleftharpoons Co^{2+}$	$E_o = 1.808 + 0.0591 \log\frac{[Co^{3+}]}{[Co^{2+}]}$	(55)
	$Co^{2+} + H_2O \rightleftharpoons CoOH^+ + H^+$	$\log\frac{[CoOH^+]}{[Co^{2+}]} = pH - 9.85$	(55,56)
11. Co^{3+}	$Co^{3+} + H_2O \rightleftharpoons CoOH^{2+} + H^+$	$\log\frac{[CoOH^{2+}]}{[Co^{3+}]} = pH - 1.78$	(55,56,57)
12. Ni^{2+}	$Ni^{2+} + 2H_2O \rightleftharpoons HNiO_2^+ + 3H^+$	$\log\frac{[HNiO_2^-]}{[Ni^{2+}]} = 3pH - 30.40$	(55,56,57)

Table 4.1 (cont'd.)

Metal Ion	Reaction	Related Information	Reference
13. Zn^{2+}	$Zn^{2+} + H_2O \rightleftharpoons ZnOH^+ + H^+$	$\log\frac{[ZnOH^+]}{[Zn^{2+}]} = pH - 9.62$	(55,56,57)
	$ZnOH^+ + H_2O \rightleftharpoons HZnO_2 + 2H^+$	$\log\frac{[HZnO_2]}{[ZnOH^+]} = 2pH - 17.97$	(55,56)

Precise values of the redox potentials for these complex compounds and polymers is not available.

A possible interpretation for the variation of the electrochemical reaction rate of V_{aq}^{3+}/V_{aq}^{2+} couple with the concentration of H^+ ion (Table 4.2) (Figure 4.1) can be given by assuming the reaction to proceed through an inner-sphere bridge mechanism. An inner-sphere activated complex reaction mechanism was previously established for a number of homogeneous redox reaction involving vanadium (II) complexes[51-54]. A feature of many of these reactions is that the rate constants and activation parameters remain essentially unaltered despite a large variation in the nature of the oxidant. Similar evidence for the homogeneous reaction of iron (II) aquo complex is not present to demonstrate the validity of the inner-sphere activation complex mechanism[51]. The kinetic rate of the reaction depends upon the energy of the activated transition state and its stability. This energy barrier height is defined by the change in the metal-ligand bound lengths during the reaction. If the aquo complex of vanadium is attached to the electrode surface via the partially positive hydrogen atom of a ligand water molecule, this bond can be assumed to be quite stable because of the relatively negative redox potential for the $V_{aq}^{3+/2+}$ couple (compare with the redox potential for $Fe_{aq}^{3+/2+}$). The presence of the bond between the aquo complex and metal electrode through the

Table 4.2 $V^{3+/2+}$ Redox Reaction at Different $[H^+]$ @ 25°C.

H^+ in M	1.0	0.1	0.02
$k_{het} \times 10^3$ cm sec^{-1} scan rate @ 50 mV/sec.	1.63	2.36	2.59
$-E_f$(mV) vs. NaSce	465	447	487

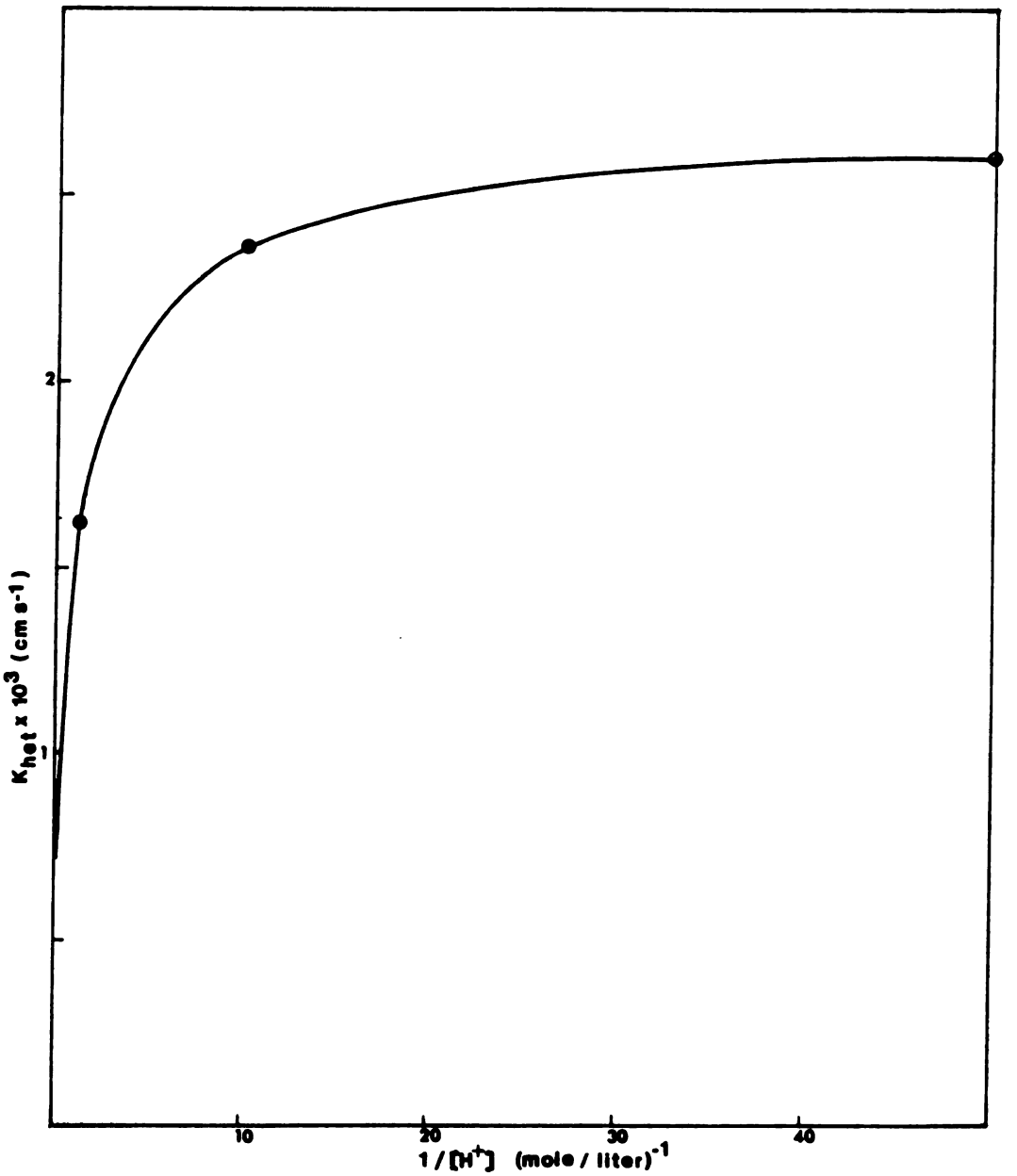

Figure 4.1. The variation of the electrochemical redox rate constant for $V^{2+}aq$ in aqueous solution with inverse hydrogen ion concentration.

hydrogen atom would decrease the height of the activated state energy profile or, in other words, it would minimize the height of the energy barrier for the reaction. The hydrolysis constant K_h of this vanadium complex would then be expected to be significantly higher than the K_h value for an ordinary homogeneous reaction, i.e., the ratio of the concentration of the unhydrolysed state to the concentration of hydrolysed product (e.g., $\log \frac{[V(H_2O)_6^{2+}]}{[V(H_2O)_5OH^+]}$ will decrease effectively for the heterogeneous reaction. Thus, the electrode surface would act as an electron donor and will assist in the hydrolysis of the vanadium aquo complex. It has been shown[55 - 58] that the hydrolysed products of vanadium, i.e., VOH^{2+} and VOH^+, have a strong tendency to form a number of polymers as well as oxo compounds. The working range of pH for the vanadium aquo complex without the formation of the hydrolysed product for a heterogeneous electrochemical reaction is thus expected to be considerably narrower than that for the corresponding homogeneous reaction; hence the reaction is expected to be sensitive to the concentration of H^+ ion in the solution even at low pH values. As the pH increases, according to the hypothesis, it facilitates the hydrolysis and helps to decrease the energy of the activated state and to stabilize it and thus, decreasing the barrier height of the activated state. The values obtained for V_{aq}^{2+} oxidation in the present work

(Table 4.2) indicate that the heterogeneous rate increases as the pH of solution increases. A negative shift in the formal potential (E_f) due to a decrease in the H^+ ion concentration indicates that there is a possibility that the precursor and successor states are hydrolysed complexes, oxo products and/or polymers.

The present work shows that the rate constants for the electrochemical redox reactions of simple transition metal aquo complex couples except vanadium are independent of the pH of solution in the working range where the complexes do not have any hydrolysed reactant. A discrepancy is found for vanadium which shows an increase rate constant with a decrease in the H^+ ion concentration. The possible explanations given in this study are not conclusive and the topic needs further investigation.

CHAPTER V

ACTIVATION PARAMETERS OF ELECTRODEPOSITION REACTIONS

A. Activation Parameters

A detailed picture of an electrochemical reaction remains incomplete without the availability of the activation energy values which are direct measures of the energy necessary for the formation of transition state, i.e., for the structural changes of the reacting particles in the course of formation of the transition state, where as an ordinary chemical rate constant is generally a composite quantity and its relation to the electronic structures of the reacting particles is not simple[10, 21, 22, 23]. The separation of reaction free energies ΔG° and free energies of activation $\Delta G^{\ddagger}$ for homogeneous chemical processes, including redox reactions, into their enthalpic and entropic components is a common procedure with a well established significance. In contrast, relatively little attention has been devoted to the corresponding enthalpic and entropic quantities for electrode reactions. One of the reasons is that several distinct electrochemical activation parameters may be defined depending on the way the electrical state of the system is controlled while the temperature

is varied[9]. This problem was discussed in detail, and it was concluded that opinions about the electrochemical activation parameters as unattainable quantities are unduly pessimistic[9].

Two experimental arrangements have been used[11, 12, 21-27]. To determine the enthalpic and entropic barrier by means of temperature dependence of the electrochemical reaction:

(i) The temperature of the cell (including the reference electrode) is varied (isothermal cell).

(ii) The temperature of the working electrode compartment including the solution is varied while the temperature of reference electrode and surrounding solutions is kept constant (non-isothermal cell).

Although both types of cell arrangements have been employed, the nonisothermal cell is preferred to the other for two reasons. First, a number of otherwise convenient reference electrodes (e.g., calomel electrodes) reestablish their equilibrium potentials very gradually after an alteration in temperature; also, the equilibrium potential does not remain the same at different temperatures, and hence one has to know the variation of this quantity with temperature. Second, by giving attention to proper cell design, the Galvani potential difference across the thermal liquid junction "ϕ_{tlj}" between the "warm" and "cold"

electrolytes can be arranged to be small and probably negligible[24-27].

When the nonisothermal cell is used and if the nonisothermal potential E^{ni} between working and reference electrode is held constant, the temperature dependence of the metal-solution Galvani potential ϕ_m will be[24-27]

$$(\frac{\partial \phi_m}{\partial T})_{E^{ni}} = -(\frac{d\phi_{tlj}}{dT} + \frac{d\phi_{tc}}{dT}),$$

where ϕ_{tc} is the "thermocouple" potential difference between "warm" and "cold" regions of the working electrode. Absolute values of $\frac{d\phi_{tc}}{dT}$ are known to be very small[28]; this coefficient is equal to about +15 $\mu V deg^{-1}$ for mercury[10]. Absolute values of $d\phi_{tlj/dT}$ can not be obtained experimentally, but there is strong evidence from a variety of sources[24-27] that this coefficient is small ($\lesssim$ 50 $\mu V deg^{-1}$) for thermal junctions formed with most electrolytes except from strong acids or bases[24]. Thus holding E^{ni} fixed while temperature is varied should hold ϕ_m constant to a very good approximation. These uncertainties prove to be essentially negligible in comparison with typical variation in redox kinetics and equilibria that are experienced as a function of temperature at the electrode solution interface. For example, an uncertainty in $(\partial \phi_m / \partial T)_{E^{ni}}$ of ± 50 $\mu V deg^{-1}$ corresponds to an uncertainty in the "ideal" entropy of activation of only ± 1 e.u.[10].

In common with other types of chemical reactions, approximate adherence to the Arrhenius relation is generally found in that ln k is linear in 1/T. Thus, the so-called "real" enthalpy and entropy of activation which are derived from the temperature dependence of the standard electrochemical rate constant are closely related to the activation parameters for the corresponding homogeneous self-exchange reactions[9]. For chemically irreversible processes for which the standard potentials are unknown, "real" parameters cannot be determined. However, it is still possible to determine the so-called "ideal" activation parameters which are obtained from the temperature dependence of the electrochemical rate constant when the metal-solution Galvani potential difference ϕ_m in all likelihood is held constant[9]. The "ideal" parameters are of particular interest because they are equal to the actual enthalpic and entropic barrier heights for the activation of a single reacting ion at the electrode potential at which they are determined.[9]. Although extra thermodynamic assumptions are inevitably involved to conclude that ϕ_m is held constant while the temperature at the electrode-solution interfaces is altered a nonisothermal cell where the reference electrode is held at a fixed temperature, it is shown earlier that these assumptions are valid to a very good approximation. This method was shown to provide useful values for the activation parameters which, in turn, were in accord with the known or

expected characteristics of their respective reactions[10, 27, 29].

In the present work, the enthalpies and entropies of activation of a special class of electrochemical reactions, called the electrodeposition reaction, were evaluated for several transition aquated metal ions in water. The reactions chosen for study can be represented as

$$M^{2+}_{aq} + 2e^- \text{ (Hg electrode, } \phi_m) \rightleftharpoons M(Hg)_{amalgum} \qquad (5.1)$$

at the mercury-aqueous interface held at a Galvani metal-solution potential difference ϕ_m, where M denotes a transition metal. The ideal enthalpic and entropic components $\Delta H^{\ddagger}_{ideal}$ and $\Delta S^{\ddagger}_{ideal}$ of the standard free energy barrier to electron transfer $\Delta G^{\ddagger}_{ideal}$ for the reaction can, in principle, be obtained directly from the temperature dependence of the electrochemical rate constants at constant ϕ_m. These parameters are related to the apparent electrochemical rate constant in the conventional form[30, 31],

$$k_{app} = Z_e \kappa\rho \exp\left(\frac{\Delta S^{\ddagger}_{ideal}}{R}\right) \exp\left(\frac{\Delta H^{\ddagger}_{ideal}}{RT}\right) \qquad (5.2)$$

where Z_e is the heterogeneous collision frequency[30, 31] and κ and ρ are constants[30, 31]. The ideal enthalpy and entropy of activiation can be separately expressed as[9]

$$\Delta H^{\ddagger}_{ideal} = R \left[\frac{\partial(\ln k_{app} - \ln T^{\frac{1}{2}})}{\partial(1/T)}\right]_{\phi_m} \qquad (5.3)$$

$$\Delta S^{\ddagger}_{ideal} = R \text{ in } k_{app} - R \ln Z_e \kappa\rho + \frac{\Delta H^{\ddagger}_{ideal}}{T} \qquad (5.4)$$

where the term $T^{\frac{1}{2}}$ in the former equation arises from the temperature dependence of the heterogeneous collision frequency Z_e [31].

The kinetic and thermodynamic results of electrodeposition reactions of transition metal ions are supposed to give additional information than that available from an ordinary redox electrochemical reaction. In ordinary electrochemical redox reactions of transition metal ions, the transfer of electrons results not only in the change of the ionic charge of the products but also in the change of ionic environment in terms of metal-ligand bond strengths and distances and the solvent structure. The values of the kinetic and thermodynamic results are expected to predict and relate the extent of these changes during the reaction. The kinetic and thermodynamic parameters thus obtained for a simple metal redox electrochemical reaction leads to the interpretation of only the relative change of the characteristics of the oxidant and reductant ions. For example, the change in the entropy of the overall reaction gives the "extent of change" of the polarization of the surrounding solvent molecules. The electrodeposition reaction, on the other hand, involves the metal particle as the reduced product. Thus, the kinetic and thermodynamic parameters of these reactions give the relative change in the reactant

characteristics with respect to an uncharged, uncomplexed and unsolvated metal particle.

B. Experimental Procedures and Analysis of Data

1 m$\underline{M}$ solutions of Mn^{2+}, Fe^{2+} and Co^{2+}, and 0.4 m$\underline{M}$ for Ni^{2+} were prepared in 0.2 $\underline{M}$, 0.5 $\underline{M}$ and 1.0 M $NaClO_4$ supporting electrolyte. Normal pulse polarography was employed using NaSCE as a reference electrode. The experiments were run at different temperatures including 25.0°C. The reference electrode was always removed from the solution while changing the temperature of supporting electrolyte. Polarograms for the supporting electrolytes were also obtained at different temperatures to cancel out the residual current for the metal ion solutions. Current vs. potential and limiting current were obtained from the polarograms after subtracting the residual current. The diffusion coefficients were obtained for each experiment using the formula.

$$D = \left(\frac{i_l}{nFAC_b}\right)^2 (A t_i) \qquad (5.5)$$

where D is the diffusion coefficient, i_l is the limiting current, n is the charge on the reacting ion, F is the Faraday constant, C_b is the concentration of the reacting ion in bulk solution, t_i is the sample time of the instrument, which was 0.048 sec., and A is the area of the drop which was calculated as

$$A = 0.8515\ (m\ t_2)_T^{2/3} \qquad (5.6)$$

where m is the natural flow rate of mercury at temperature T through the capillary in g/sec. and t_2 is the drop time of the knocker. Since the natural flow rate of mercury at the dropping mercury electrode changes with temperature, it was necessary to determine the quantity at different temperatures. This experiment was arranged by dipping the tip of the DME about 2 inches in a container filled with water and kept at constant temperature. The amount of mercury passed through the capillary which was held at known temperature for a known amount of time was determined after drying it free of water at low temperature. The experiment was run at different temperatures ranging from 0°C to 60°C and a graph was plotted for the flow rate versus temperature.

The data was analyzed to give k_{app} values versus the potential[32]. The rate constants k_{corr} vs. potential were calculated using the formula

$$\log k_{corr} = \log k_{app} - \frac{F}{2 \cdot 3RT} (\alpha_{corr} - Z_r)\phi_r \qquad (5.7)$$

α_{corr} is obtained from the relation

$$\text{corr} = \frac{\alpha_{app} - Z_r(\partial\phi_r/\partial E)_\mu}{1 - (\partial\phi_r/\partial_E)\mu} \qquad (5.8)$$

where Z_r is the ionic charge of the reducing ion, and ϕ_r is the potential of the reaction site which is assumed to be equal to ϕ_2 obtained from GCS theory. The values of ϕ_2 can be usually found in the literature for sodium fluoride at the mercury aqueous interface at 25°C and at

different ionic strengths at different potentials[34, 35]. No suitable data is available to estimate this quantity at different temperatures. However, Grahame[33] has obtained capacitance potential data for sodium floride ion as a function of temperature and electrolyte concentration. From these plots, q^m vs. the "relative" Galvani potential difference across the inner layer at different temperatures was obtained[10]. These plots, it was assumed, should be almost identical for fluoride and perchlorate electrolytes at the negative potential of interest $\lesssim$ 800 mV since percholorate anions are adsorbed only to a small extent under these conditions. The values of q^m at different temperatures and ionic strengths were obtained from the above mentioned plots for 0.8 M sodium fluoride electrolyte solution at different temperature using the following method. Plots for q^m vs. temperature for each potential in the working range were obtained; then from these plots, q^m was plotted vs. potential for each experimental working temperature. Values were obtained in this way for 0.8 M NaF electrolyte. The values of q^m vs. potential at different ionic strengths were obtained from the values of q^m vs. ϕ_2 calculated from the GCS model[2] for 0.8 M and other concentrations of supporting electrolyte at the temperature of interest. The differences in ϕ_2 values for each q^m in both concentrations were obtained and these values were subtracted from the applied potential values of the 0.8 M NaF q^m vs.

potential plot, at that temperaure, for concentrations lower than 0.8 M (i.e., 0.5 M and 0.2 M), and added for concentrations greater than 0.8 M. This gave data for new plots of q^m vs. potential and these plots were then, in turn, used to determine ϕ_2 values at different potentials at each ionic strength at each temperature. The apparent activation enthalpy was determined by plotting ($\ln k_{app} - \ln T^{\frac{1}{2}}$) vs. 1/T, the slope of which was multiplied by -R to give the value of the desired quantity $\Delta H_i^{\ddagger}$ according to equation[9] 5.3. The apparent activation entropy was determined at 25°C using equation 5.4.

The value for the corrected enthalpy $\Delta H^{\ddagger}_{corr}$ was determined by first plotting ϕ_2 vs. 1/T for each ionic strength and the values for the respective slopes were used in the equation

$$\Delta H^{\ddagger}_{corr} = \Delta H^{\ddagger}_{ideal} + \frac{F}{T}\{(\alpha_{corr} - Z_r)[\partial\phi_2/\partial(1/T)_{\phi_m}]\} \quad (5.9)$$

The values obtained for $\Delta H^{\ddagger}_{corr}$ were used to determine $\Delta S^{\ddagger}_{corr}$ using equation (5.4). The values of $\Delta G^{\ddagger}_{corr}$ were obtained from the equation

$$\Delta G^{\ddagger}_{corr} = RT(\ln k_{corr} - \ln Z_e) \quad (5.10)$$

where $Z'_e = 5 \times 10^3$ cm s^{-1}.

C. Results and Discussion

The electrodeposition reduction kinetics of Mn^{2+}, Fe^{2+}, Co^{2+} and Ni^{2+} aquo complexes at the mercury-aqueous interface were studied as a function of temperature within

a range of 0 - 60°C. "Ideal" enthalpies of activation $\Delta H^{\neq}_{ideal}$ were determined from the dependence of the apparent electrochemical rate constants k_{app} (i.e., uncorrected for ionic double-layer effects) as a function of temperature at a constant non-isothermal cell potential E^{ni} (and hence, at essentially constant ϕ_m) by using equation 5.3. These "Arrhenius" plots were usually found to be linear over the full temperature range 0 - 60°C. "Ideal" entropies of activiation $\Delta S^{\neq}_{ideal}$ were determined from the corresponding values of $\Delta H^{\neq}_{ideal}$ along with the values of k_{app} measured at 25°C using equation 5.4. The resulting values of $\Delta H^{\neq}_{ideal}$ and $\Delta S^{\neq}_{ideal}$, as well as k_{app} determined at 25°C at few working potentials vs. NaSCE are summarized in Tables 5.1 - 5.4.

All the reactions were carried out with the reactant concentration of 1 m$\underline{M}$ except for the nickel reaction for which the concentration 0.4 m$\underline{M}$ was observed to avoid polarographic maxima and possibly slow electrocrystallization at the mercury surface. Reactions were carried out in three concentrations of supporting electrolyte (0.2 $\underline{M}$, 0.5 $\underline{M}$ and 1.0 $\underline{M}$) to study the effect of the diffuse layer and the double-layer correction. The electrolyte was chosen to be $NaClO_4$, since specific absorption from this electrolyte is small or negligible at the negative electrode potential at which these aquo complexes are reduced, and since the magnitude of the double-layer effects is relatively small under these conditions.

Table 5.1. Manganese: $Mn^{2+/0}$ (1m$\underline{M}$) reduction reaction.*

-E(mV)	$k_{app} \times 10^4$ cm s^{-1}	$k_{corr} \times 10^4$ cm s^{-1}	$\Delta H^{\ddagger}_{ideal}$ k cal mol^{-1}	$\Delta H^{\ddagger}_{corr}$ k cal mol^{-1}	$\Delta S^{\ddagger}_{ideal}$ cal deg^{-1} mol^{-1}	$\Delta S^{\ddagger}_{corr}$ cal deg^{-1} mol^{-1}	$\Delta G^{\ddagger}_{corr}$ k cal mol^{-1}	conc. of supporting electrolyte $\underline{M}$	
1500	55.9	15.9	15.6	14.9	25.0	20.1	8.9	0.2	α_{app}=1.67
1450	2.2	0.6	17.3	16.6	24.3	19.6	10.8	0.2	α_{corr}=1.66
1400	8.3×10^{-2}	2.5×10^{-2}	18.7	18.1	23.6	19.1	12.7	0.2	
1500	57.9	15.3	15.2	14.5	23.9	19.6	8.9	0.5	α_{app}=1.58
1450	2.7	0.73	16.4	15.7	21.8	17.6	10.7	0.5	
1400	12.4×10^{-2}	3.5×10^{-2}	17.7	17.0	20.0	16.0	12.5	0.5	α_{corr}=1.56
1500	59.7	14.0	14.6	13.7	21.6	16.7	8.9	0.75	α_{app}=1.46
1450	3.5	0.9	14.1	13.4	14.7	10.0	10.6	0.75	
1400	2.0×10^{-2}	5.2×10^{-2}	13.8	13.0	7.8	3.3	12.3	0.75	α_{corr}=1.44
1500	64.3	16.0	14.6	13.8	22.1	16.7	8.8	1.0	α_{app}=1.45
1450	3.8	0.99	14.3	13.57	15.2	10.3	10.5	1.0	
1400	22.4×10^{-2}	6.1×10^{-2}	13.9	13.2	8.3	3.5	12.2	1.0	α_{corr}=1.43

*Values given for 25°C.

Table 5.2. Iron: $Fe^{2+/0}$ (1.0m$\underline{M}$) reduction reaction.*

-E(mM)	$k_{app} \times 10^4$ cm s^{-1}	$k_{corr} \times 10^4$ cm s^{-1}	$\Delta H^{\ddagger}_{ideal}$ k cal mol^{-1}	$\Delta H^{\ddagger}_{corr}$ k cal mol^{-1}	$\Delta S^{\ddagger}_{ideal}$ cal deg^{-1} mol^{-1}	$\Delta S^{\ddagger}_{corr}$ cal deg^{-1} mol^{-1}	$\Delta G^{\ddagger}_{corr}$ k cal mol^{-1}	conc. of supporting electrolyte $\underline{M}$	
1500	1710	9.9	17.1	14.2	36.9	17.1	9.1	0.2	α_{app}=0.73
1450	416	2.7	16.2	13.4	31.0	11.9	9.9	0.2	
1400	101	0.8	15.3	12.6	25.1	6.6	10.7	0.2	α_{corr}=0.66
1350	24.7	0.2	14.3	11.8	19.2	1.1	11.4	0.2	
1500	673	9.6	15.7	13.6	30.3	14.9	9.2	0.5	α_{app}=0.59
1450	186	3.0	14.9	12.7	25.2	9.6	9.8	0.5	
1400	51.7	0.9	14.1	11.9	20.0	4.4	10.5	0.5	α_{corr}=0.66
1350	14.3	0.3	14.5	11.1	15.4	- 0.3	11.2	0.5	
1500	202	5.4	14.9	12.9	25.2	11.4	9.5	1.0	α_{app}=0.58
1450	65.5	2.0	14.4	12.5	21.5	8.0	10.1	1.0	
1400	21.3	0.7	14.0	12.2	17.9	5.1	10.7	1.0	α_{corr}=0.52
1350	6.9	0.3	13.6	11.9	14.3	2.1	11.3	1.0	

Values given for 25°C.

Table 5.3. Cobalt: $Co^{2+/0}$ (1.0m$\underline{M}$) reduction reaction.*

-E(mV)	$k_{app} x10^4$ cm s^{-1}	$k_{corr} x10^4$ cm s^{-1}	$\Delta H^{\ddagger}_{ideal}$ k cal mol^{-1}	$\Delta H^{\ddagger}_{corr}$ k cal mol^{-1}	$\Delta S^{\ddagger}_{ideal}$ cal deg^{-1} mol^{-1}	$\Delta S^{\ddagger}_{corr}$ cal deg^{-1} mol^{-1}	$\Delta G^{\ddagger}_{corr}$ k cal mol^{-1}	conc. of supporting electrolyte $\underline{M}$	
1450	1176	6.1	16.9	14.0	35.4	15.3	9.4	0.2	α_{app}=0.60
1400	368	2.2	16.6	13.8	32.0	12.6	10.0	0.2	
1350	115	0.8	16.3	13.6	28.7	9.9	10.6	0.2	α_{corr}=0.52
1300	360	0.3	15.8	13.3	25.0	6.8	11.2	0.2	
1450	323	3.0	15.3	12.7	27.7	9.7	9.9	0.5	α_{app}=0.48
1400	127	1.3	15.5	13.1	26.6	9.2	10.3	0.5	
1350	49.7	0.6	15.8	13.4	25.5	8.8	10.8	0.5	α_{corr}=0.40
1300	19.5	0.3	16.1	13.8	24.8	8.7	11.2	0.5	
1450	163	4.7	14.6	12.7	23.8	10.3	9.6	1.0	α_{app}=0.50
1400	61.9	2.0	14.9	13.0	22.8	9.8	10.1	1.0	
1350	23.5	0.9	15.1	13.4	21.8	9.4	10.6	1.0	α_{corr}=0.43
1300	8.9	0.4	15.4	13.8	20.8	9.0	11.1	1.0	

*Values given for 25°C.

Table 5.4. Nickel: $Ni^{2+/0}$ (0.4m$\underline{M}$) reduction reaction.*

-E(mV)	$k_{app} x10^4$ cm s^{-1}	$k_{corr} x10^4$ cm s^{-1}	$\Delta H^{\neq}_{ideal}$ k cal mol^{-1}	$\Delta H^{\neq}_{corr}$ k cal mol^{-1}	$\Delta S^{\neq}_{ideal}$ cal deg^{-1} mol^{-1}	$\Delta S^{\neq}_{corr}$ cal deg^{-1} mol^{-1}	$\Delta G^{\neq}_{corr}$ k cal mol^{-1}	conc. of supporting electrolyte $\underline{M}$	
1100	15.5	4.3	15.9	14.1	28.0	15.1	9.6	0.2	α_{app}=0.79
1050	33.4	1.1	16.5	14.9	27.2	14.8	10.5	0.2	
1000	7.2	0.3	17.2	15.7	26.4	14.9	11.3	0.2	α_{corr}=0.69
950	1.6	$7.4x10^{-2}$	17.9	16.5	25.7	15.0	12.1	0.2	
1100	199	8.0	16.4	15.2	30.2	19.9	9.3	0.5	α_{app}=0.80
1050	11.7	2.0	16.9	15.7	28.9	18.8	10.1	0.5	
1000	8.7	0.5	17.4	16.3	27.4	18.0	10.9	0.5	α_{corr}=0.72
950	1.8	0.1	18.0	17.0	26.3	17.6	11.7	0.5	
1100	303.4	39.9	17.2	16.2	33.8	26.5	8.3	1.0	α_{app}=0.83
1050	60.3	8.9	17.5	16.6	31.6	24.7	9.2	1.0	
1000	11.9	2.0	17.8	17.0	29.4	23.1	10.1	1.0	α_{corr}=0.76
950	2.4	0.45	18.1	17.3	27.1	21.2	11.0	1.0	

*Values given for 25°C.

Even in these concentrated electrolytes, the effects of the ionic double-layer upon $\Delta H^{\ddagger}_{ideal}$ and $\Delta S^{\ddagger}_{ideal}$ are not quite negligible. In order to interpret these activation parameters in terms of ion-solvent interactions, it is desirable to correct them for the "double-layer" effects which arise from long-range Coulombic interactions between the reacting species and its environment within the interphasial region. The double-layer effects were accounted for by calculating a rate constant k_{corr} according to equation 5.7. Estimates of $\Delta G^{\ddagger}_{corr}$ were also compiled according to equation 5.10. Additionally, estimates of the effect of the ionic double layer on $\Delta H^{\ddagger}_{ideal}$, calculated earlier, were obtained to give the "double-layer corrected" ideal enthalpy of activiation $\Delta H^{\ddagger}_{corr}$. These values were used to calculate the corresponding values of $\Delta S^{\ddagger}_{corr}$. All these values are summarized in Tables 5.1--5.4 along with the "apparent" and "double-layer corrected" transfer coefficients. The corrected transfer coefficient α_{corr} was calculated from the slope of ln k_{corr} vs. applied potential according to the equation

$$\alpha_{corr} = - \frac{R}{T}(\partial \ln k_{corr} / \partial E)_{T,\mu} \qquad (5.11)$$

Aside for the dependence of $\Delta H^{\ddagger}_{corr}$ and $\Delta S^{\ddagger}_{corr}$ upon the reactant charge and atomic environment at a given electrode potential, an additional characteristic of interest could be to evaluate the enthalpic and entropic contributions to variation of $\Delta G^{\ddagger}_{corr}$ with varying potential.

These contributions can, in principle, be separated by studying the temperature dependence of the electrochemical transfer coefficient[10]. Combining equations 5.10 and 5.11, the potential dependence of k_{corr} can be expressed as[10]

$$-\frac{RT}{F}(\partial \ln k_{corr}/\partial E)_{T,\mu} = \partial\Delta G^{\ddagger}_{corr}/\partial\Delta G^{o}_{rc} = \alpha_{corr} \qquad (5.12)$$

and thus

$$\partial\Delta G^{\ddagger}_{corr}/\partial\Delta G^{o}_{rc} = (\partial\Delta H^{\ddagger}_{corr}/\partial\Delta G^{o}_{rc}) - T(\partial\Delta S^{\ddagger}_{corr}/\partial\Delta G^{o}_{rc}) \qquad (5.13)$$

correspondingly,

$$\alpha_{corr} = (\partial\Delta H^{\ddagger}_{corr}/\partial\Delta G^{o}_{rc}) - T(\partial\Delta S^{\ddagger}_{corr}/\partial\Delta G^{o}_{rc}) = \alpha^{H}_{corr} + \alpha^{S}_{corr} \qquad (5.14)$$

where ΔG^{o}_{rc} is the free energy change for the reduction reaction, α^{H}_{corr} and α^{S}_{corr} are the components of α_{corr} associated with the variation of $\Delta H^{\ddagger}_{corr}$ and $\Delta S^{\ddagger}_{corr}$, respectively, with varying electrode potential. Hence, if α_{corr} is independent of absolute temperature, the contribution of α^{H}_{corr} to the potential-dependence of the reaction rate would be dominant, whereas if α_{corr} is proportional to temperature, α^{S}_{corr} will have the dominant contribution. Table 5.2 summarizes the experimental results for the temperature dependence of α_{app} within the range of experimental potentials.

Since the entropy of conduction electrons in metals is in all probability negligibly small,[51] the entropy driving

force ΔS^{o}_{rc} should be contributed solely by the changes in the Coulombic double-layer effects and/or reactant-solvent interactions[59]. Moreover, the so-called "intrinsic" contribution to the potential dependence of the electrochemical rate constant denoted by the intrinsic transfer coefficient α_I[60], which arises from variations in the Fermi level of the metal electrode vs. the energy level of the reacting ion in bulk solution (i.e., variation in the free energy of the reacting electron), should be purely enthalpic in origin. On the other hand, the so-called "environmental" part α_E of the measured transfer coefficient α_{app} which arises from differences in the interaction between the reacting particle and its environment at the interphase compared with those of the bulk solution, may be enthalpic and/or entropic in origin. The correction of α_{app} for Coulombic double-layer effects, by using equation 5.8 to yield values of α_{corr} accounts for some, but possibly not all, of this environmental term α_E. Thus, changes in ion-solvent interactions with varying electrode potential that might arise from changes in interphasial solvent interactions can lead to differences between α_{corr} and α_I.

The mechanism of electrodeposition reaction for the transition metal aquo complexes was shown to occur first through a dissociation reaction of one or more of the coordinated water molecules[61-64]. It has been proposed that the resulting ion, which may be regarded as activated

intermediate responds to the coordination unsaturation by forming a bond with the metal atom on the electrode surface having excess electronic charge. The surface cathodic process can be represented as[64]:

$$E + M^{(z)}(H_2O)_p \rightleftharpoons E - M^{(z)}(H_2O)_q + (p-q)(H_2O) \qquad (5.14)$$

$$E - M^{(z)}(H_2O)_q + Z_e \rightleftharpoons E - M^{(o)}(H_2O)_q \qquad (5.15)$$

$$E - M^{(o)}(H_2O)_q \rightleftharpoons E - M^{(o)} + q(H_2O) \qquad (5.16)$$

where E is the electrode metal, M is the reducing metal ion with oxidation state z and p and q are the coordination numbers of the metal ion.

The extent of bonding between the reacting metal ion bonded to the water molecule and the metal atom depends upon the Fermi level of the electrode surface and the energy of the available vacant orbitals on the activated intermediate. The extent of coordination of the water molecules to the activated intermediate, as a consequence, depends on the electrode potential and the individual characteristics of the reacting metal ion.

Dependence of activation entropy $\Delta S^{\ddagger}_{corr}$ on electrode potential

The experimental results obtained for the transfer coefficient α_{app}, summarized in Table 5.5, clearly indicate a direct dependence on the temperature which can be interpreted as $\alpha^{S}_{corr} > \alpha^{H}_{corr}$, i.e., the dependence of entropic

Table 5.5. The variation of the electrochemical transfer coefficient with temperature at different ionic strengths for the electrodeposition reaction of some transition metal aquo complexes in water at mercury-aqueous interface.

Mn^{2+}

0.2 M $NaClO_2$		0.5 M $NaClO_4$		1.0 M $NaClO_4$	
Temp. °C	α_{app}	Temp. °C	α_{app}	Temp. °C	α_{app}
4.4	1.63	3.4	1.53	1.8	1.35
14.4	1.64	16.2	1.54	11.8	1.24
25.0	1.67	25.0	1.58	25.0	1.45
34.9	1.66	36.1	1.60	36.0	1.52
46.2	1.64	46.2	1.58	46.2	1.54

Fe^{2+}

3.5	0.61	34.0	0.54	3.2	0.53
13.3	0.66	14.8	0.63	14.2	0.54
25.0	0.73	23.3	0.67	25.0	0.58
25.5	0.73	25.0	0.66	36.7	0.62
36.0	0.78	36.0	0.70	48.7	0.68
36.0	0.82	46.6	0.74		

Co^{2+}

3.0	0.53	4.6	0.51	1.3	0.49
9.3	0.50	9.6	0.51	12.3	0.49
16.9	0.50	16.3	0.52	25.0	0.50
25.0	0.60	25.0	0.48	36.0	0.52
32.6	0.61	36.4	0.54	46.0	0.52
41.0	0.64	46.2	0.56		

Ni^{2+}

12.8	0.75	11.9	0.74	16.4	0.78
25.0	0.79	25.0	0.80	25.0	0.83
36.1	0.78	36.2	0.81	36.1	0.82
46.2	0.77	46.1	0.82	46.2	0.84

component $\Delta S^{\neq}_{corr}$ on the electrode potential which is the observed for almost all of the couples. This result also is consistent with the assumption that the reaction proceeds through an activated intermediate partially bonded to the electrode surface; since the increase in the cathodic electrode potential will enhance the extent of activated intermediate-to-electrode bonding, on the other hand, decreasing the extent of bonding between the ligand water molecules and the metal ion, consequently, increasing the activation entropy of the reaction. One parameter which may, however, reduce the activation entropy is the partial bonding between the metal ion and the electrode surface or the partial solvation of the metal ion in the mercury electrode liquid. The variation of activation entropies with the change of supporting electrolyte concentration is directly in relation with the change in the transfer coefficient. The experimental results can be compared with the absolute entropies of the aqueous ions (Table 5.6) to give a rough comparative estimate of the extent of desolvation of the intermediate.

The activation enthalpy contributions are within an experimentally reasonable range of ± 1 k cal/mole in a working potential range of 200 mV for the solution containing 1 M of supporting electrolyte. A larger variation in the activation enthalpy with a change in potential is observed for lower ionic strengths, except for the activation enthalpy

Table 5.6. Entropy of some transition metal aqueous ions according to Powell and Latimer.

	$\bar{S}°$/e.u.
Mn^{2+}	-20.0
Fe^{2+}	-27.1
Co^{2+}	-27.1
Ni^{2+}	-24.9

Entropy of aqueous ion determined using Powell and Latimer[65], using the formula $\bar{S} = \frac{3}{2} R \ln M + 37 - 270 \frac{Z}{r_e^2}$ where M is the atomic weight, Z is the absolute value of the charge of the ion, and r_e is the effective ionic radius + 2.00 A, assuming the true ionic entropy of hydrogen ion as zero. The values for r_e are taken from Pauling's crystal radii[66].

of cobalt which does not show any appreciable variation. The reason for this potential dependence of activiation enthalpy can be interpreted as the improper assumption that ϕ_r is equal to ϕ_2 calculated from the GCS model.

The charge transfer process for the ions except manganese shows that first electron transfer is rate determining, while for mangenese the second electron transfer is rate determining. This is clear from looking into the effective charge on the activated intermediate which is equal to $(Z_r - \alpha_{corr})$[67]. The existence of univalent ionic intermediates for Mn, Fe, Co and Ni is supported by the pulse radiolysis reduction reactions for their corresponding +2 oxidation states[68]. The reactions, according to their transfer coefficient α_{corr}, are not far from having a symmetrical barrier at higher ionic strength (i.e., 1 M, except for Mn^{2+} and Ni^{2+} which show a higher transfer coefficient.

BIBLIOGRAPHY

1. W.J. Albery. "Electrode Kinetics," Clarendon Press, Oxford, 1975, Chapter 1.

2. P. Delahay, "Double Layer and Electrode Kinetics," Interscience, New York, 1965, Chapter 39.

3. A.J. Bard and L.R. Faulkner, "Electrochemical Methods - Fundamentals and Applications," John Wiley, 1980, Chapter 12.

4. B.E. Conway, "Theory and Principles of Electrode Processes," Ronald, New York, 1965.

5. F.C. Anson and B.A. Parkinson, J. Electroanal. Chem., 85, 317 (1977).

6. A.R. Sears and F.C. Anson, loc. cit., 47, 521 (1973).

7. P.D. Tyma and M.J. Weaver, J. Electroanal. Chem., 111, 195 (1980).

8. M. Temkin, Zh. Fiz, Khim., 22, 1081 (1948).

9. M.J. Weaver, J. Phys. Chem., 80, 2645 (1976).

10. M.J. Weaver, loc. cit., 83, 1748 (1979).

11. A.A. Vleck, Collect. Czech. Chem. Commun., 24, 3538 (1959).

12. R. Tamamushi, Rev. Polarog., 10, 1 (1962).

13. J. Koutecky, Collect. Czech. Chem. Commun., 18, 597 (1953).

14. J. Weber and J. Koutecky, loc. cit., 20, 980 (1955).

15. K.B. Oldham and E.P. Parry, Anal. Chem., 38, 867 (1966).

16. R.S. Nicholson, loc. cit., 37, 1351 (1965).

17. M.J. Weaver and F.C. Anson, J. Electroanal. Chem., 84, 47 (1977).

18. R. Payne, Trans. Faraday Soc., 64, 1638 (1968).

19. M.J. Weaver and F.C. Anson, J. Electroanal. Chem., 65, 711 (1975).

20. K. Niki and H. Mizota, loc. cit., 72, 307 (1976).

21. R.E. Powell and W.M. Lakimer, J. Chem. Phys., 19, 1139 (1951).

22. J.W. Cobble, loc. cit., 21, 1446 (1953).

23. P. George, G.I. Hanania, and D.H. Irvine, 1616 (1954).

24. A.J. deBethune, T.S. Licht, N. Swendenian, J. Electrochem. Soc., 106, 616 (1959).

25. A.J. deBethune, loc. cit., 107, 829 (1960).

26. E.D. Eastman, J. Am. Chem. Soc., 50, 292 (1928).

27. E.L. Yee, R.J. Cave, K.L. Guyer, P.D. Tyma and M.J. Weaver, loc. cit., 101, 1131 (1979).

28. J.N. Agar in "Advances in Electrochemistry and Electrochemical Engineering," Vol. 3, P. Delahay, Ed., Interscience, New York, 1963, Chapter 2.

29. M.J. Weaver, J. Phys. Chem., 84, 568 (1980).

30. R.A. Marcus, Can. J. Chem., 37, 155 (1959).

31. R.A. Marcus, J. Chem. Phys., 43, 679 (1965).

32. K.B. Oldham and E.P. Parry, Anal. Chem., 40, 65 (1968).

33. D.C. Grahame, J. Am. Chem. Soc., 79, 2093 (1957).

34. D.C. Grahame, J. Am. Chem. Soc., 76, 4821 (1954).

35. C.D. Russell, J. Electroanal. Chem., 6, 490 (1963).

36. A.N. Frumkin, Z. Phys. Chem., 164A, 121 (1933).

37. For a recent review, see P.P. Schmidt in Electrochemistry - A specialist Periodical Report, Vol. 5, The Chemical Society, 1975, Ch. 2; Vol. 6, 1977, Ch. 4.

38. R. Parsons and E. Passeron, J. Electroanal. Chem., 12, 525 (1966).

39. D.M. Mohilner, J. Phys. Chem., 73, 2652 (1969).

40. F.C. Anson, N. Rathjen and R.D. Frisbee, J. Electrochem. Soc., 117, 477 (1970).

41. T. Dickinson and D.H. Angell, J. Electroanal. Chem., 35, 55 (1972).

42. K. Suga, J. Mizota, Y. Kaneaki and S. Aoyagi, J. Electroanal. Chem., 41, 313 (1973).

43. P. Bindra, A.P. Brown, M. Fleishmann and D. Pletcher, J. Electroanal. Chem., 58, 39 (1975).

44. J.M. Saveant and D. Tessier, J. Electroanal. Chem., 65, 57 (1975).

45. M.J. Weaver and F.C. Anson, J. Phys. Chem., 80, 1861 (1976).

46. J.M. Saveant and D. Tessier, J. Phys. Chem., 81, 2192 (1977).

47. Z. Samec and J. Weber, J. Electroanal. Chem., 77, 163 (1977).

48. D.A. Corrigan and D.H. Evans, J. Electroanal. Chem., 106, 287 (1980).

49. R. Parsons, Croat. Chem. Acta, 42, 281 (1970).

50. D.R. Crow, Polaragraphy of Metal Complexes, Academic Press, London, 1969.

51. R.N.F. Thorneley and A.G. Sykes, J. Chem. Soc. (A), 1036 (1970).

52. N. Sutin, Accounts Chem. Res., 1, 225 (1968).

53. J.M. Malin and J.H. Swinehart, Inorg. Chem., 7, 250 (1968).

54. W. Kruse and D. Thusius, Inorg. Chem., 7, 464 (1968).

55. M. Pourbaix, Ed., "Atlas of Electrode Equilibrium in Aqueous Solution," Pergamon, London, 1966.

56. L.G. Sillen and Martell, Ed., "Stability Coefficient of Metal-ion Complex," Sp. Publ. 17, Chem. Soc., London, (1964); and its suppl. #1, (1971).

57. R.M. Smith and A.E. Martell, Ed., "Critical Stability Constant," V. 4, Plenum, New York (1976).

58. J. Kragten, Ed., "Atlas of Metal-Ligand Equilibria in Aqueous Solution," Wiley, New York, (1978).

59. N.F. Mott and H. Jones, "The Theory of the Properties of Metals and Alloys," Oxford University Press, London, 1936, Chapter 6.

60. R. Parsons, Croat. Chim. Acta, 42, 281 (1970).

61. E.H. Lyons, Jr., J. Electrochem. Soc., 101, 363 (1954).

62. E.H. Lyons, Jr., J. Electrochem. Soc., 101, 376 (1954).

63. A.J. Band, Ed., "Encyclopeadea of Electrochemistry," v. III, p. 276.

64. V.I. Kravtsov, Elektrokhimiya, 9, 1702 (1973).

65. R.E. Powell and W.M. Latimer, J. Chem. Phys., 19, 1139 (1951).

66. L. Pauling, "The Nature of the Chemical Bond," Cornell University Press, New York (1939).

67. P.D. Schmidt in "Electrochemistry - A Specialist Periodic Report," vol. 5, The Chemical Society, London, 1975, Chapter 2.

68. J.H. Baxondale and R.S. Dixon, Z. Physik, Chem. Neue Folge, 43, 161 (1964).